TU Delft

Delft University of Technology

Document Version
Final published version

Licence
CC BY

Citation (APA)
Abdel-Raouf, Y. M. A., Maes, L., Maga, L., De Backer, J., Sips, P., Peirlinck, M., Famaey, N., Humphrey, J. D., & Segers, P. (2026). The role of vascular smooth muscle cell plasticity in arterial remodelling and biomechanical failure: a numerical approach. *Proceedings of the Royal Society A: Mathematical, Physical and Engineering Sciences*, *482*(2336), Article 20250787. https://doi.org/10.1098/rspa.2025.0787

Important note
To cite this publication, please use the final published version (if applicable).
Please check the document version above.

Copyright
In case the licence states “Dutch Copyright Act (Article 25fa)”, this publication was made available Green Open Access via the TU Delft Institutional Repository pursuant to Dutch Copyright Act (Article 25fa, the Taverne amendment). This provision does not affect copyright ownership.
Unless copyright is transferred by contract or statute, it remains with the copyright holder.

Sharing and reuse
Other than for strictly personal use, it is not permitted to download, forward or distribute the text or part of it, without the consent of the author(s) and/or copyright holder(s), unless the work is under an open content license such as Creative Commons.

Takedown policy
Please contact us and provide details if you believe this document breaches copyrights.
We will remove access to the work immediately and investigate your claim.

This work is downloaded from Delft University of Technology.

PROCEEDINGS A

royalsocietypublishing.org/journal/rspa

CC BY

Research

Cite this article: Abdel-Raouf YMA, Maes L, Maga L, De Backer J, Sips P, Peirlinck M, Famaey N, Humphrey JD, Segers P. 2026 The role of vascular smooth muscle cell plasticity in arterial remodelling and biomechanical failure: a numerical approach. *Proc. R. Soc. A* **482**: 20250787.
https://doi.org/10.1098/rspa.2025.0787

Received: 12 September 2025
Accepted: 12 February 2026

Subject Areas:
biomedical engineering, mathematical modelling, computer modelling and simulation

Keywords:
osteochondrocytic phenotype, maladaptation, glycosaminoglycans, elastin, hypertension, aneurysm, smooth muscle cell

Author for correspondence:
Yousof M. A. Abdel-Raouf
e-mail:
yousofmohammadasaad.abdelraouf@ugent.be

Electronic supplementary material is available online at https://doi.org/10.6084/m9.figshare.c.8351677.

THE ROYAL SOCIETY PUBLISHING

The role of vascular smooth muscle cell plasticity in arterial remodelling and biomechanical failure: a numerical approach

Yousof M. A. Abdel-Raouf[1], Lauranne Maes[1,3], Ludovica Maga[4], Julie De Backer[2,5], Patrick Sips[2], Mathias Peirlinck[4], Nele Famaey[3], Jay D. Humphrey[6,7] and Patrick Segers[1]

[1]Institute of Biomedical Engineering—BioMMedA, and [2]Center for Medical Genetics Ghent, Department of Biomolecular Medicine, Ghent University, Ghent, Belgium
[3]Biomechanics Section, Department of Mechanical Engineering, KU Leuven, Leuven, Belgium
[4]Department of BioMechanical Engineering, Delft University of Technology, Delft, The Netherlands
[5]Department of Cardiology, Ghent University Hospital, Ghent, Belgium
[6]Department of Biomedical Engineering, Yale University, New Haven, CT, USA
[7]Vascular Biology and Therapeutics Program, Yale School of Medicine, New Haven, CT, USA

YMAAR, 0009-0008-2544-3963; LM, 0000-0002-1192-0836; PS, 0000-0003-3870-3409; MP, 0000-0002-4948-5585; NF, 0000-0002-7374-8912; JDH, 0000-0003-1011-2025

Vascular smooth muscle cell (VSMC) plasticity is implicated in extracellular matrix (ECM) turnover and arterial failure. The osteochondrocytic phenotypes of synthetic VSMCs are thought to drive glycosaminoglycan (GAG) accumulation and swelling typically seen in connective tissue disease and hypertension. A central question is whether

© 2026 The Authors. Published by the Royal Society under the terms of the Creative Commons Attribution License http://creativecommons.org/licenses/by/4.0/, which permits unrestricted use, provided the original author and source are credited.

Downloaded from http://royalsocietypublishing.org/rspa/article-pdf/doi/10.1098/rspa.2025.0787/6133611/rspa.2025.0787.pdf
by TU Delft user
on 08 May 2026

this phenotype switching under non-homeostatic conditions is a cause or effect of those conditions. We implement a cause–effect association between ECM damage, lost cell mechanosensitivity, and cell phenotype modulation using the Constrained Mixture Model, to simulate the evolution of VSMC population over time. We modelled a cylindrical bi-layer of media and adventitia of a mouse common carotid artery and simulated remodelling in response to initially compromised ECM, concurrent with varying degrees of hypertension. In normo- and moderately hypertensive ECM disruption, physiological remodelling restores mechanical homeostasis to cells with slightly altered mechanical properties. Alternatively, severe hypertension yields complete medial degeneration. Complete loss of stored elastic energy is observed, with stiffened arteries yielding characteristically high pulse wave velocities (PWVs). Early intervention recovering hypertensive to normotensive pressure, as well as enhanced adventitial collagen turnover, are shown to prevent medial degeneration. Our model thus offers a tool to better understand the relationship between ECM damage, arterial failure, and hypertension.

1. Introduction

The extracellular matrix (ECM) serves as a dynamic structural framework that not only provides mechanical support to soft tissues, such as large elastic arteries, but also plays a critical role in cellular signalling and environmental sensing [1,2]. Central to arterial adaptation and maladaptation is the architecture of the medial layer of large elastic arteries, where vascular smooth muscle cells (VSMCs) are embedded in concentric elastin lamellae, interspersed with collagen and glycosaminoglycans (GAGs) as well as other signalling and regulatory molecules. Effective VSMC mechanosensing depends on anchorage to elastic fibre extensions that transduce mechanical signals to the cell [3,4]. In fibrillar form, elastin anchors cells to lamellae and mediates force transfer; in lamellar form, it provides structural integrity and communication pathways during development, forming load-bearing sheets [5]. However, elastin synthesis and cross-linking largely cease after early childhood, effectively resulting in the elastin lamellae having a half-life of 70 years [6]. Their degradation with ageing, along with compensatory collagen deposition, leads to arterial stiffening, hypertension [7,8], and is associated with aortic aneurysms (AAs) or aortic dissections (ADs) [9–11].

Elastin damage may have several underlying causes; in ageing it results from lamellar fatigue (possibly accelerated by hypertension) [12,13], while in genetic disorders it stems from defective structural components. In Marfan syndrome (MFS), for example, mutation of the elastin associated glycoprotein fibrillin-1 reduces lamellar integrity, promoting vessel dilatation and AA/AD [14]. Likewise, a deficiency in normal fibulin-4, another elastin-associated glycoprotein, can cause AA [13]. Indeed, disrupted TGF-beta signalling (mutations to genes encoding ligands, receptors, and downstream signalling molecules) in Loeys–Dietz Syndrome (LDS) has comparable effects [10,11].

Like elastin, collagen plays a key role in maintaining aortic homeostasis when functional, and disease when dysregulated. Its turnover increases with ageing [15] and hypertension [16], while deficient collagen contributes to AA in genetic disorders like vascular Ehlers–Danlos Syndrome (vEDS) [10,17]. Kawamura *et al.* highlight that the adventitia and its physiologically robust collagen are essential protections from rupture in VSMC dysregulated aortas [18], and Weiss *et al.* show that AA formation requires combined adventitial collagen disruption (via BAPN), elastin degradation, and GAG accumulation—not any single factor alone [19]. In human AA, Yousef *et al.* report that tissue composition is a reliable indicator for diagnosing asymptomatic aneurysm, with increased GAGs and VSMCs and reduced elastin being most significant contributors [20]. Imaging and biomechanical tests show that collagen becomes thicker and straighter in elastase-treated mice [21]. Combined with increased cross-linking [17], this results in lower material stiffness but higher structural stiffness due to increased collagen deposition.

Downloaded from http://royalsocietypublishing.org/rspa/article-pdf/doi/10.1098/rspa.2025.0787/6133611/rspa.2025.0787.pdf
by TU Delft user
on 08 May 2026

While previously overlooked in regards to arterial biomechanics, GAGs also have an important role in mechanosensing; they influence interlamellar spacing (and fibrillar elastin stretch) by sequestering water molecules in a phenomenon called *Donnan swelling*, facilitating mechanosensing of embedded VSMCs [22]. Hyaluronan and proteoglycans (PGs) like versican are common in healthy arteries, whereas aggrecan and fibronectin increase in AA [10]. In ageing, an increase in interlamellar distance, with a decrease in distension throughout cardiac pulsation, suggests that the moderately accumulated GAGs and swelling work to maintain this interlamellar distance [23,24]. An extreme case is Hutchinson-Guilford Progeria Syndrome, where VSMCs adopt an osteochondrogenic phenotype and overproduce GAGs, though the triggers remain unclear [25]. This leads to ECM detachment, dysfunction and anoikis (a form of programmed cell death). It has been observed that GAG build-up and swelling increases viscous energy loss in abdominal AA throughout the cardiac cycle [26], suggesting that ECM swelling and damage—not diameter alone—may serve as interesting biomarkers for arterial disease. Furthermore, increased GAG build-up with upregulated cell turnover has been reported in carotid arteries of hypertensive mouse models [27,28].

Computational models have provided critically-needed insights into these disease phenomena. Li *et al.* show that elastin degradation and impaired mechanosensing together, not separately, are necessary to reproduce aneurysm formation [29]. Maes *et al.* demonstrate how mechanobiological feedback models can simulate maladaptation under hypertensive conditions [30]. Notably, Roccabianca *et al.* explicitly model GAG swelling within a constrained mixture framework, showing that moderate osmotic loading improves compliance, while excess impairs energy storage [31,32]. Murtada *et al.* further model GAG accumulation and its consequences in progeroid mice [33]. These works offer insight into the mechanical role that GAGs play in the arterial space, but a relation coupling the presence of GAGs to VSMCs, and the more rapid GAG producing osteochondrocytes, remains lacking. The simultaneous remodelling of these constituents, as well as elastin degradation and collagen turn-over, is not described to date, and less so is one that associates the biomechanical consequences of VSMC phenotype switching that occurs ubiquitously in hypertension [10,11], diabetes mellitus [34] or atherosclerosis [35]. To this end, our study aims to consolidate the concepts explored in the large body of work presented beforehand in a strongly coupled computational framework. Evidence suggests that VSMC phenotype switching from the contractile to the synthetic and progressively to the osteochondrocytic phenotype, and excess GAG production associated with this new phenotype, may be a mechanism by which medial degeneration occurs [25,35]. What we present in this work is a numerical framework that relates these concepts, extending the work of Roccabianca *et al.* [31,32]. By investigating the hypothesis that VSMC maladaptation results primarily from disrupted mechanosensing due to elastin fibre damage, which triggers compensatory GAG production, our model aims to clarify the mechanistic pathways underlying arterial degeneration and provide insights into potential therapeutic strategies for arterial diseases.

2. Methods

Our computational approach has two distinct parts: the first describes the Biomechanics model that describes the biomechanical response of arterial tissue to physiological and supra-physiological loading conditions subject to the mechanical conservation laws of nature. We adopt the continuum-based hyperelastic material model and convention largely presented in Roccabianca *et al.* and Sorrentino *et al.* [31,32]. The second part is the Constituent Evolution model, and elucidates the mechanobiological response and behaviour at these loads, largely representing the phenomenological observations made on *in vivo* cellular adaptation. Since adaptation is a process subject to time and initial perturbation (referred to as an insult), we will initially perturb our model from what we assume is a homeostatic environment, and then observe—given the severity of the insult—how the cell response will play out.

Downloaded from http://royalsocietypublishing.org/rspa/article-pdf/doi/10.1098/rspa.2025.0787/6133611/rspa.2025.0787.pdf
by TU Delft user
on 08 May 2026

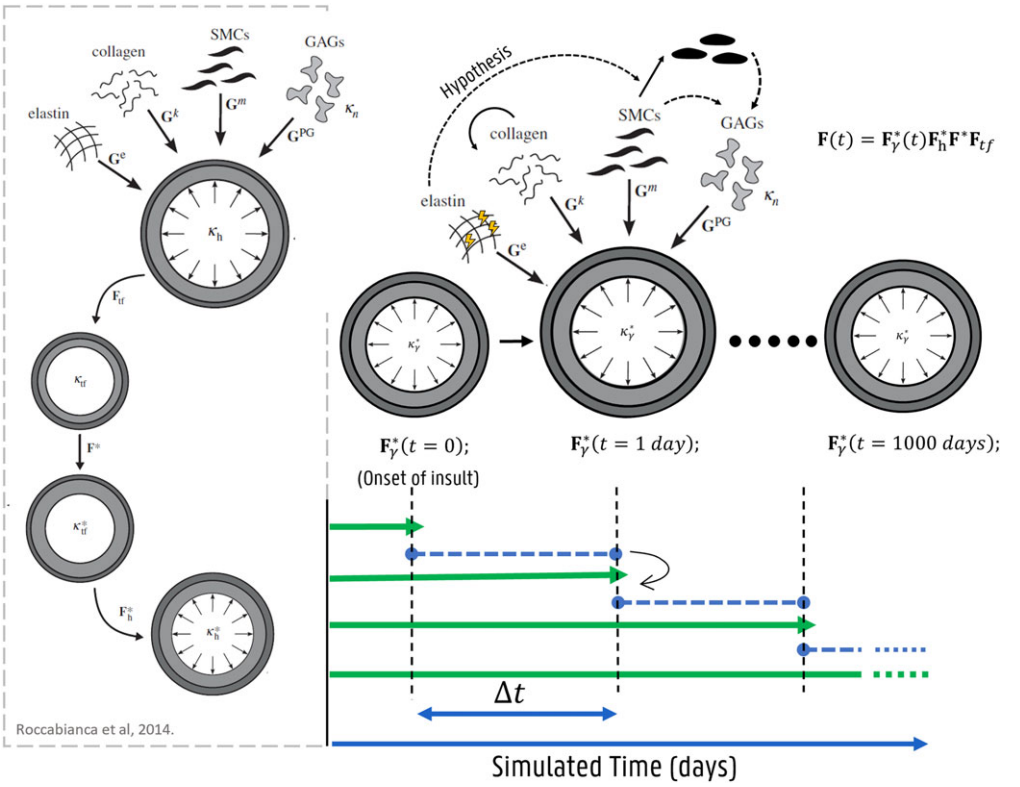

Figure 1. A schematic of configurations of interest. Configurations κ_h and κ_h^* correspond to non-swollen *in vivo* and swollen *in vivo* homeostatic configurations respectively. When $\mathbf{F^*} = \mathbf{I}$, these configurations are identical, and similarly for the traction-free (κ_{tf}) and swollen traction free (κ_{tf}^*) configurations. κ_γ^* represents new hypothetical configurations of adaptation at time $t = 0$, and configurations transform from κ_h^* to κ_γ^* through the deformation gradient $\mathbf{F}_\gamma^*$. Throughout this work, all quantities denoted with a subscript '*h*' refer to a homeostatic configuration (at κ_h^*), while a subscript '0' refers to a value at initial configuration of insult (κ_γ^*) at time $t = 0$. In colour: a schematic to determine configurations over time. The boundary value problem (BVP), shown in solid green arrows and described in §2a, dictates that configurations of interest satisfy quasi-static equilibrium, while the initial value problem (IVP) described in §2b is shown in dashed blue. Given a deformation $\mathbf{F}_\gamma^*$ at time t, the resulting biomechancical values are used as initial conditions, and the IVP is solved on discrete time interval (Δt). The resulting parameters at the end of the time frame $t + \Delta t$ are used as boundary conditions on the BVP, and a new deformation $\mathbf{F}_\gamma^*$ is estimated that satisfies the governing equation.

(a) Biomechanical model

In order to estimate the biomechanical characteristics of arterial tissue at different stages of loading and adaptation, we utilize a computational model of a bilayered, idealized cylindrical common carotid artery composed of a media (comprising approximately 38% of the total thickness *in vivo*) and an adventitia. The layers are modelled as constrained mixtures of anisotropic hyperelastic continua [36], with axial pre-stretch of 1.7 obtained at an intraluminal mean arterial pressure corresponding to a systolic pressure of 120 mmHg and a diastolic pressure of 80 mmHg [31,37]. (This corresponds to a mean arterial pressure of $80 + (120 - 80)/3$ which will be labeled henceforth as 93 mmHg). The mixture deforms uniformly by $\mathbf{F}$ and because independent constituents, referred to as α, are assumed to be pre-stretched from a stress-free configuration by $\mathbf{G}^{\boldsymbol{\alpha}}$, the final constituent-specific deformations are thus given by $\mathbf{F}^{\boldsymbol{\alpha}} = \mathbf{F}\mathbf{G}^{\boldsymbol{\alpha}}$. As illustrated in figure 1, we examine the configurations of interest going from a homeostatic configuration (κ_h) to a swollen configuration at *in vivo* conditions (κ_h^*). Insults will create a new

Downloaded from http://royalsocietypublishing.org/rspa/article-pdf/doi/10.1098/rspa.2025.0787/6133611/rspa.2025.0787.pdf
by TU Delft user
on 08 May 2026

configuration (κ_γ^* at time $t = 0$), after which swelling and cell adaptation take place. Henceforth, we use the subscripts 'h' and 'γ' to refer to homeostatic and damaged/adapted/maladapted configurations, respectively, and a superscript '*' to indicate whether or not swelling is accounted for.

(i) Governing equations and boundary value problem

We assume deformation, swelling, growth and remodelling occur quasi-statically, where the governing equation is

$$\nabla \cdot \boldsymbol{\sigma} = \mathbf{0}, \tag{2.1}$$

where $\boldsymbol{\sigma}$ is the Cauchy stress.

The equation is solved over the domain of the two layers of the artery, with Neumann Boundary Conditions corresponding to $\sigma_{rr}(r_i) = P_{iv}$, where P_{iv} is the *in vivo* hemodynamic pressure and $\sigma_{rr}(r_i)$ is the radial component of the Cauchy stress at the luminal surface (corresponding to the inner surface of the domain at r_i). On the outer surface (at r_o) of the domain, the Boundary Condition corresponds to $\sigma_{rr}(r_o) = 0$. Finally, we impose the condition of axisymmetry, with the force due to axial prestretch on the domain being $\boldsymbol{f} = [0, 0, f_z]$.

(ii) Kinematics

Central to our model is the assumption that an initial insult perturbs the condition of the artery from a biomechanical, homeostatic equilibrium. Henceforth, we assume this equilibrium to be the *in vivo* configuration at which axial pre-stretch is prescribed, namely κ_h (figure 1). Kinematically, we define a transformation from this configuration to a new one that occurs due to insult or adaptation κ_γ^*. The mapping between these two configurations is defined in the electronic supplementary material, Extended Methods i, and the deformation gradient between these mappings is $\mathbf{F}_{\boldsymbol{\gamma}}^{*} = \mathrm{diag}[\mathrm{d}r_\gamma^*/\mathrm{d}r, r_\gamma^*/r, 1]$, where $\nu_\gamma^* = \det(\mathbf{F}_{\boldsymbol{\gamma}}^{*})$ is the volume change as a result of swelling, and r_γ^* is the radius at this new configuration. We assume that no configurations produce volume change except for the adapted one κ_γ^*, as seen in figure 1, where $\nu = \nu_\gamma^* = J = \det(\mathbf{F}_{\boldsymbol{\gamma}}^{*})$. This is a departure from the values obtained from osmotic loading in Sorrentino *et al.* and Roccabianca *et al.*, and henceforth traction-free osmotic loading between configurations κ_{tf} and κ_{tf}^* is ignored (i.e. $\mathbf{F}^* = \mathbf{I}$).

While all deviation from homeostasis and subsequent adaptation or maladaptation takes place on a temporal scale, we emphasize the assumption that all deformations due to these adaptations are quasi-static, such that no viscous or inertial effects occur. We also assume that cell and matrix turnover in the media is uniform, noting that the diffuse nature of GAG accumulation and swelling is in line with clinically observed specimens [32].

(iii) Constrained mixture model

The biphasic model assumes four distinct biomechanical load-bearing constituents, namely the elastin, VSMC, GAG and collagen with the former three having a significantly larger mass fraction in the media compared to the adventitia, and the latter having the opposite distribution. In this mixture, the VSMCs involved in the biomechanical load-bearing are those of the contractile phenotype. We utilize the model presented in Roccabianca *et al.* and Murtada *et al.* to describe the constrained mixture and GAG strain energy functions [25,31], and present it in the electronic supplementary material, Extended Methods section ii.

Volume change of the biphasic mixture here (defined as ν) occurs primarily due to Donnan Swelling and the presence of GAGs [38]. Essentially, we relate the current mass, or for convenience referential mass fraction of GAGs (φ^G) to the volume change J, and the osmotic pressure (Π) due to Donnan swelling [33,39,40]. We describe these constitutive relations between osmotic pressure and volume change more explicitly in the electronic supplementary material, Extended Methods ii. The load-bearing role of GAGs is elaborated on in §2biii.

Downloaded from http://royalsocietypublishing.org/rspa/article-pdf/doi/10.1098/rspa.2025.0787/6133611/rspa.2025.0787.pdf
by TU Delft user
on 08 May 2026

To summarize the above in the context of our study: the evolution of constituent mass fractions and tissue volume (due to swelling) will dictate the deformations ($\mathbf{F}^*_\gamma$) for which the governing equation of quasi-static equilibrium (equation (2.1)) is satisfied. The next section will outline the phenomenological growth and remodelling laws proposed to determine this temporal evolution, and present a numerical means to characterize several key biological phenomena.

(b) Constituent evolution model

The Constrained Mixture Model (CMM) offers a unique opportunity to examine the impact of each constituent in the mixture on the total strain energy given the ratio they occupy in the mixture and how they individually deform [41]. To that effect, and utilizing the previous statement of the CMM in electronic supplementary material, equation A.2, we present the following relation between the current constituent-specific strain energy, referential mass fractions and total strain energy:

$$W_{Rt} = \frac{\sum \varphi^\alpha_{Rt}}{J} \sum (\varphi^\alpha_{Rt} W^\alpha_t), \tag{2.2}$$

where W^α_t is the current constituent-specific strain energy and φ^α_{Rt} represents the current mass fraction of constituent α with respect to the original total mass. We show how we obtained equation (2.2) in the electronic supplementary material, Extended Methods i. The use of this expression becomes clear when defining rates of evolution that are first order (i.e. $\dot{m}^\alpha = f(\Upsilon, m^\alpha, t)$) but we lack information about the total mass, only initial mass fractions. All subsequent rates of that form are thus assumed to be in total reference mass, and thus $\dot{m}^\alpha \simeq \dot{\varphi}^\alpha_{Rt}$, i.e. we omit the subscript Rt in the following formulation.

(i) Elastin damage models

Two distinct roles of medial elastin are explored. We distinguish the damage that affects elastin in its lamellar configuration (γ^l), which is the primary load-bearing mechanism in the media, and the damage to elastin fibers (γ^f) that are assumed to connect VSMCs to their extracellular environment.

Lamellar elastin damage

Deformation of the elastin lamellae is what is directly accounted for in the Constrained Mixture ($\varphi^e \sigma^e$ in electronic supplementary material, equation A12), and it is assumed that the interlamellar elastic fibers are a negligible factor and carry no stress in mechanical load-bearing but a major role in mechanosensing. Here, temporal evolution of consequent damage to elastin lamellae is assumed to be driven by stress felt on those structures due to distension

$$\frac{\mathrm{d}\gamma^l}{\mathrm{d}t} = k^l_\gamma \Delta\sigma^e(\gamma^l)(1-\gamma^l), \tag{2.3}$$

where $\Delta\sigma^e$ is defined as the deviation of the elastin-specific stress from a homeostatic value, explicitly as $\Delta\sigma^e = \mathrm{tr}(\boldsymbol{\sigma}^e)/\mathrm{tr}(\boldsymbol{\sigma}^e_h) - 1$ for all values of $\Delta\sigma^e > 0$. k^l_γ is a constant that defines the sensitivity to stress deviation. This stress driven damage is then limited to values $0 < \gamma^l \leq 1$ and is strictly increasing, consistent with the features of elastin lamellae that cannot be repaired past early development. With the rate described in equation (2.3) being strictly positive, we also highlight the immediate damage that occurs in excess stress, without any delay associated with this event. This damage is then accounted for in the load bearing as a depletion of the elastin constituent mass fraction:

$$\varphi^e = (1-\gamma^l)\varphi^e_h. \tag{2.4}$$

The choice of incorporating damage in the mass ratio term is deliberate, and its implication is that damage depletes load-bearing elastin, not the intrinsic ability of elastin lamellae to bear loads. We explore in electronic supplementary material, appendix ii the difference between incorporating

Downloaded from http://royalsocietypublishing.org/rspa/article-pdf/doi/10.1098/rspa.2025.0787/6133611/rspa.2025.0787.pdf
by TU Delft user
on 08 May 2026

damage of lamellae in the term φ^e or in c^e. Note that the initial value of damage, γ_0^l, in subsequent simulations is assumed to be the main perturbation from homeostasis. This event is what we consider the insult, or the onset of maladaptation. The physical meaning behind this value underscores whether insult and maladaptation can be impacted heavily at different ages, since elastin damage correlates with age.

Elastic fibre damage

The second consideration focuses on interlamellar elastic fibrils (elastin plus elastin-associated glycoproteins including fibrillin-1) attaching cells to their environment. This is a simplification of the biological struts that often involve many proteins including TGF-β binding complexes and integrins [2,42]. All these molecules act as an ensemble offering a distensible quality to these cell–ECM connections, and focal adhesion complexes then act as mechanoreceptors to stress along these ensembles, globally referred to as elastic fibers or elastic fibrils. As swelling causes medial expansion and thickening, the stretch pushing apart lamellar layers will create tensile stresses that act to stretch the elastic fibers. Damage (γ^f) evolves according to a similar principle to the lamellar damage as below

$$\frac{\mathrm{d}\gamma^f}{\mathrm{d}t} = k_\gamma^f \cdot \Gamma(\varepsilon_r) \cdot \left(1 - \frac{\gamma^f}{\varphi^s/\varphi_h^s}\right), \tag{2.5}$$

where $\Gamma(\varepsilon_r)$ defines the progression of damage due to stretch of the fibers, and φ^s and φ_h^s define the mass of VSMCs in the current and homeostatic configurations, respectively. Since independent fibers are diffuse, and distributed arbitrarily in the circumferential direction, the radial component is the primary axis of sensing interlamellar distance. Thus the thickness of the media is correlated to that interlamellar distance, and elastic fibre damage progression is coupled to deviation of interlamellar thickness. Radial stretch is measured as $\varepsilon_r = (\tau - \tau_h)/\tau_h$ (where τ is medial thickness and τ_h is thickness at homeostasis). The progression is then related back to the thickening (due to swelling) in interlamellar spaces, and a lower limit for radial stretch ($\varepsilon_{r_{\mathrm{crit}}}$) beyond which interlamellar elastin is torn is then defined. Damage initiation is then defined at a critical stretch beyond 80% and up to 220% [43], i.e. $\Gamma = (\varepsilon_r - \varepsilon_{r_{\mathrm{crit}}})/(\varepsilon_{r_{\max}} - \varepsilon_{r_{\mathrm{crit}}})$ for $\varepsilon_r \geq 0.8$, and $\Gamma = 0$ for $\varepsilon_r < 0.8$. As we designate the stretch at which we expect damage to occur, we create a demarcation in our model where the maladaptive process is fully assumed to take effect. By dividing the damage parameter γ^f with the VSMC mass gain (φ^s/φ_h^s), we account for the appearance of new cells with full mechanosensitive integrity, and the buffering effect this may have on accumulation of mechanosensitive damage.

It is important to consider that this arrangement of damage implies—similar to that of equation (2.3)—that elastic fibers of individual cells are not replenished once they are damaged, only being replenished by the appearance of new cells. Furthermore, the assumption that the overall medial thickening impacts all fibers across the media is discussed more closely in the discussion section.

Values of constants used to simulate elastin lamellar damage and elastic fibre damage can be found in electronic supplementary material, table A1.

(ii) Contractile VSMC turnover and osteochondrogenic phenotype

In consideration of the load bearing constituents of the ECM, we model contractile VSMC turnover, as well as production of GAGs and collagen. These cells work to restore sensed stresses to a preferred homeostatic value, and accordingly, we incorporate the constrained mixture model with terms describing rates of production and removal of contractile VSMCs, as well as those of the osteochondrogenic phenotype in the media are, as follows

$$\frac{\mathrm{d}\varphi^m}{\mathrm{d}t} = k^m \Delta\sigma^m \varphi^m - K^{\mathrm{mal}} \varphi^m \varphi^o \tag{2.6}$$

and

$$\frac{\mathrm{d}\varphi^o}{\mathrm{d}t} = K^{\mathrm{mal}} \varphi^m \varphi^o - k^{\mathrm{anoi}} \Delta\rho^o \varphi^o; \tag{2.7}$$

Downloaded from http://royalsocietypublishing.org/rspa/article-pdf/doi/10.1098/rspa.2025.0787/6133611/rspa.2025.0787.pdf
by TU Delft user
on 08 May 2026

where once again $\Delta\sigma^m$ is defined as the perturbation from homeostatic stress due to tension on contractile VSMCs, and subject to sensed stresses through elastic fibers where $\Delta\sigma^m = [(1-\gamma^f)\cdot \sigma^m/\sigma_h^m] - 1$, for all $\Delta\sigma^m > 0$. The populations of cells are referred from their mass fractions where φ^m and φ^o are the referential mass fractions of contractile and osteochondrocytic phenotypes of VSMCs in a given volume of media, respectively. The gain parameters k^m, K^{mal} and k^{anoi} represent the parameters governing stress-driven VSMC growth rate, damage driven phenotype switch, and anoikis rate, respectively.

We introduce the term $\Delta\rho^o$ in equation (2.7) that describes anoikis: phenomenon of death or loss of cell viability in the medial environment due to excessive degradation of the ECM leading to a loss of cell–cell and cell–matrix interactions. Since the growth of osteochondrocyte population is pathological, we define the two roles of this growth. In the first term, we account for the effect of osteochondrocytes overcrowding contractile VSMCs, and in the second, we account for the resultant high density and excess amount of osteochondocytic cells. This is implemented in the medial volume numerically as $\Delta\rho^o = ((\varphi^o/\varphi^s)(\varphi_h^s/\varphi_h^o))\cdot([J^{-1}\cdot(\varphi^o/\varphi_0^o)] - 1)$. Anoikis is then driven by this density coinciding with lost VSMC cell density, as well as a gain parameter indicating a basal rate k^{anoi}.

Finally, we comment on the term representing the maladaptive differentiation of VSMCs from the contractile to the osteochondrocytic phenotype. When estimating the rate of differentiation as $K^{\text{mal}}\varphi^m\varphi^o$, we incorporate the presence of pathological osteochondrocytes, as well as contractile VSMCs in the driving factors increasing phenotype switching with the underlying assumption that–next to ECM dysregulation–it takes osteochondrocyte crowding, and anoikis of surrounding VSMCs to trigger the switch.

ECM damage and lost mechanosensitivity as drivers for phenotype switch

We implement the gain parameter K^{mal} in equation (2.6) to incorporate elastin fibre and lamellar damage as $K^{\text{mal}} = k^{\text{mal}}\ (w_1\gamma^f + w_2\gamma^l)$. In the presence of osteochondrocytes in their vicinity, elastin lamellar damage and elastic fibre damage thus scale the inherent likelihood of differentiation (k^{mal}) of VSMCs, and for our studies, we choose to emphasize the tendency to differentiation on lost mechanosensitivity–or loss of anchoring of VSMCs–compared to lost lamellar integrity. Thus, we interpret parameters w_1 and w_2 as the weight due to lost mechanosensitivity on phenotype switching rate, and the weight due to lost elastin lamellae integrity on phenotype switching rate, respectively. Hence, the choice of $w_1 = 0.8$ and $w_2 = 0.2$. Values of constants used in simulating cell turnover can be found in electronic supplementary material, table A2.

(iii) GAG turnover and Gibbs-Donnan swelling

We relate the presence of GAGs in the media to their production by VSMCs, as well as rapid production of GAGs by the osteochondrogenic phenotype. We also account for GAG removal due to basal degradative processes involving proteases or similar inflammatory responses [44]. The equation that governs the presence of GAGs is as follows

$$\frac{\mathrm{d}\varphi^G}{\mathrm{d}t} = K^G\ (\eta(\eta - \varphi^G) - k^G(\varphi^G)^2), \tag{2.8}$$

where K^G and k^G correspond to a gain parameter for production and VSMC-independent removal, respectively.

Furthermore, η represents the production of GAGs by cells scaling a basal production rate (η_0) by a factor yielding $\eta = \eta_0\cdot\eta_1$. Here, $\eta_1 = 0$ corresponds to an absence of cells, therefore an absence of GAG producers, and equation (2.8) has a strictly negative loss term to deplete GAGs. We choose a function where $\eta_1 = 1$ will yield a pole or equilibrium point where the GAGs correspond to the homeostatic value, therefore we define $\eta_0 = 2\varphi_0^G/(\sqrt{5}-1)$. An illustration of the rate of GAG production and its change relative to VSMC and osteochondrocytes is shown in

Downloaded from http://royalsocietypublishing.org/rspa/article-pdf/doi/10.1098/rspa.2025.0787/6133611/rspa.2025.0787.pdf
by TU Delft user
on 08 May 2026

electronic supplementary material, figure A.3a. Accordingly, with the stated restrictions on the function η_1, a suitable description can be found as

$$\eta_1 = \frac{\exp[k^{\eta_1}(\varphi^m + k^o\varphi^o)] - 1}{\exp[k^{\eta_1}(\Delta\lambda_r \cdot \varphi_0^m + k^o\varphi_0^o)] - 1}; \tag{2.9}$$

where we let $k^o = 10$ to reflect that osteochondrogenic cells produce GAGs 10 x as rapidly as VSMCs. The presence of $\Delta\lambda_r$ in the denominator reflects the role of GAGs as a mechanism to maintain interlamellar distance, as compression of the media in the radial direction serves to then shift equilibrium GAGs in the media even at a homeostatic VSMC population.

The above allows us to define GAG production by cells, with a net accumulation when $\eta_1 > 1$ and a net removal for $\eta_1 < 1$ while also maintaining that no GAGs are produced unless these cells are present. Values of constants used to simulate GAG turnover can be found in electronic supplementary material, table A.3.

(iv) Collagen turnover in the adventitia

Collagen turnover is governed by stress-driven stimuli. The production and removal is thus governed by the following relation

$$\frac{\mathrm{d}\varphi^{c_j}}{\mathrm{d}t} = k^c\,(\Delta\sigma^{c_j})\varphi^{c_j} \tag{2.10}$$

where $\Delta\sigma^{c_j}$ defines the change in stress along collagen fibre of family j. The collagen constituent in our continuum approach encompasses the families of collagen III predominantly found in media of elastic arteries, with type I found in the adventitia. Since rapid collagen turnover is associated with decreased overall collagen integrity, new collagen produced is characterized by thicker singular fibers that are less crimped but with denser cross-linking between adjacent ones [19,24]. Phenomenologically, this change in the microstructure of the fibre network is accounted for in a loss of continuum fibre stiffness represented by parameter $k_1^{c_j}$ in electronic supplementary material, equation A8. A measure of 100% is defined for collagen produced at lower stimulus ($\Delta\sigma^{c_j}$) with an inverse correlation between integrity and stress fold-change (shown schematically in electronic supplementary material, figure A.4), and the minimum value of integrity defined at 5% at a 5-fold change of fibre stress ($CDQR = 5$). Stated numerically, the integrity (q) of fibre j is defined

$$q^j = 100\% \quad \Delta\sigma^{c_j} \leq 0 \tag{2.11a}$$

$$q^j = \left[100 - 95\left(\frac{\Delta\sigma^{c_j}}{CDQR}\right)\right]\% \quad 0 < \Delta\sigma^{c_j} \leq CDQR \tag{2.11b}$$

and

$$q^j = 5\% \quad CDQR < \Delta\sigma^{c_j}. \tag{2.11c}$$

The integrity of produced collagen at time t (q_t^j) is then added to previous collagen and the total integrity ($q_{\Sigma t}^j$) is calculated as the weighted average according to

$$q_{\Sigma t}^j = q_t^j(\varphi_t^{c_j} - \varphi_{t-1}^{c_j}) + q_{t-1}^j(\varphi_{t-1}^{c_j}) \tag{2.12}$$

with the fibre stiffness then adjusted to the new integrity relative to homeostatic stiffness $k_{1_h}^{c_j}$ as

$$k_1^{c_j} = q_{\Sigma t}^j k_{1_h}^{c_j}. \tag{2.13}$$

Values of constants used in simulating collagen turnover can be found in electronic supplementary material, table A.4.

(c) Hypothesis and overview of simulated scenarios

In this section, we illustrate the described modelling approach of coupling the mechanically constrained problem with the growth and remodelling laws assumed in figure 1.

Downloaded from http://royalsocietypublishing.org/rspa/article-pdf/doi/10.1098/rspa.2025.0787/6133611/rspa.2025.0787.pdf
by TU Delft user
on 08 May 2026

We assume mechanical homeostasis at equilibrium for a mean arterial pressure of 93 mmHg, corresponding to systolic/diastolic pressure of 120/80 mmHg, and this framework is applied to a model vessel representative of the mouse common carotid artery. We explore the hypothesis that elastin damage and lost mechanosensitivity of VSMCs drives cell differentiation, and the loss of the contiguous contractiles further disrupts cell–cell connections triggering anoikis and increasing osteochondrocytic phenotype density.

An abrupt/immediate insult is applied on the lamellae and a time scheme advances to simulate adaptation under varying degrees of hypertension. As such, there are two triggers perturbing from homeostasis: **initial insult to the elastic constituent** of the artery in the media, and **increased luminal pressure**. At every time Δt, a swelling is applied, and mass fractions are updated according to stimuli and deviations from homeostasis in the previous time step. Thus, a new static equilibrium is satisfied, and these deviations in turn dictate a new set of stimuli. This scheme is run for a cycle of 1000 days, solving for equilibrium at each 1 day and the transient response in this period reaches an equilibrium by then. The cycle of 1000 days is assumed to be adequate for any equilibrium to be reached. The radius (r_γ^*) at every time point is determined by minimizing the cost function that enforces force balance using a non-linear least squares optimization scheme (lsqnonlin, [45]), while the values of evolving constituents are solved for the subsequent time step using fourth-order Runge-Kutta solver (ode45, [45]). We demonstrate the behaviour of the model in four distinct scenarios:

— **Scenario 1: Remodelling under insult and moderate hypertension**. In this scenario, we individually simulate constituent turn-over and remodelling under normotension (purely due to insult), and various grades of moderate hypertension. In this case, an arbitrary initial insult corresponding to moderate lamellar damage ($\gamma_0^l = 15\%$) (eg. due to ageing or lamellar fatigue) is applied, and adaptation is simulated under conditions of mean Arterial Pressures corresponding to sys/dias pressures of 120/80 mmHg (93 mmHg), 130/85 mmHg (100 mmHg), 140/90 mmHg (106 mmHg) and 150/95 mmHg (113 mmHg).
— **Scenario 2: Remodelling under insult and severe hypertension**. We explore what our model can simulate with the same degree of initial elastin lamellar fragmentation ($\gamma_0^l = 15\%$), at a more moderate hypertension with a systolic/diastolic pressures of 160/100 mmHg and a mean pressure of 120 mmHg.
— **Scenario 3: Intervention and recovery by reducing hypertension**. The starting point for this scenario are the results from **scenario 2**. Consequently, we observe what happens if the pressure is relieved from the hypertensive 120 mmHg to normotensive 93 mmHg at different time points. This is to simulate the effect of intervention that reduces hypertension in a patient and the impact of intervention time.
— **Scenario 4: Intervention and recovery by enhancing adventitial response**. This is a replication of **scenario 2**, with the assumption that turnover of collagen that happens in the adventitia (i) takes place more rapidly. This constitutes an adjustment of the gain parameter in equation (2.10) (i.e. $k^c = k^m$ instead of $k^c = 1/70$ in **scenario 2**). The second aspect of enhanced adventitial integrity can be implemented when collagen turnover (ii) takes place with deposited collagen having more robustness. Here the decline in collagen deposition quality in equation (2.11) is modified (i.e. $CDQR = 100$ instead of $CDQR = 5$ in **scenario 2**). This is akin to intervention strategies that promote adventitial integrity.

We report constituent turnover in these scenarios, as well as calculated damage due to insult and subsequent (mal)adaptation. We also report evolving vessel dimensions and subsequent intramural elastic and osmotic stresses, and perform a hypothetical 'excision' and biaxial Pressure-Distension test on the evolving *in silico* model at days 50, 300 and 900 post onset of insult. Finally, we use the Bramwell-Hill equation to compute pulse wave velocities (PWVs) from Pressure-Distension relations of the evolving arteries in these scenarios [46].

Downloaded from http://royalsocietypublishing.org/rspa/article-pdf/doi/10.1098/rspa.2025.0787/6133611/rspa.2025.0787.pdf
by TU Delft user
on 08 May 2026

3. Results

(a) Scenario 1: remodelling under insult and moderate hypertension

Our simulation demonstrates key features of physiological adaptation post-insult (figure 2). The model predicts an initial progression of damage to the elastin lamellae post insult (panel a). Like the fraying of individual strands of rope, excess stress causes the lamellae to progressively disintegrate, and varying degrees of moderate hypertension cause this progression to occur more rapidly (as seen by the arrow demonstrating this trend). Turnover of contractile VSMCs and collagen (shown in figure 2b,e, respectively) have worked to reduce the stresses on the lamellae and *recover* elastin to sub-critical stress as seen by the plateau (or arrest) of elastin damage in panel (a) reached after 31, 29, 27 and 25 days in 93 mmHg, 100 mmHg, 106 mmHg and 113 mmHg pressures, respectively. As the VSMCs continue to turnover due to elevated stress compensating for the lost elastin, the sustained lamellar damage (18.04%, 19.71%, 20.89% and 21.99%) drives osteochondrocyte development, and the accompanying GAG production causes swelling (figure 2c,d, respectively). We demonstrate the trend of more rapid response at higher pressures, with similar asymptotic masses of contractile VSMCs, osteochondrocytic cells and GAGs in the long term, and more permanent differences in elastin and collagen content at these varying pressures.

The long-term evolution simulated by our model suggests recovered contractile VSMC populations (seen in panel (b)), albeit to a smaller sizes compared to ones prior to insult. The mechanosensitivity of cells also remains largely undisrupted as seen in panel (d) and this absence of damage to mechanosensitivity maintains contractile VSMC phenotypic integrity. Here, the biomechanical characteristics of the artery remain largely unchanged as evident in the Pressure-Distension of arteries at normotension and moderate hypertension remain largely similar across the range of pressures and at operational pressure at which the vessels adapted (dashed lines in panels (a) and (b) for normotensive and moderately hypertensive cases, respectively). Lasting effects of remodelling from sustained moderate hypertension include permanent elastic energy loss with stored elastic energy in the media dropping from a homeostatic 124.70 kPa before insult, to 107.68 kPa and 109.59 kPa with onset of insult at normotensive and moderately hypertensive pressures, respectively, and reduction to 102.26 kPa and 98.69 kPa by day 1000 of adaptation as shown in panel (c) (figure 3). Furthermore, it is evident that adaptation at this mild hypertension yields mildly stiffer vessels, with long-term PWVs remaining approximately $1.237 \pm 0.217\,\mathrm{m\,s^{-1}}$ higher in mild hypertension than those adapted at normotension with insult, and $1.858 \pm 0.429\,\mathrm{m\,s^{-1}}$ higher than homeostatic PWV (of $7.249\,\mathrm{m\,s^{-1}}$), as reported in table 1.

(b) Scenario 2: remodelling under insult and severe hypertension

Initial remodelling follows the same trend of contractile VSMC and adventitial collagen turnover, with GAG build-up (and thus swelling) due to the presence of the former constituent within the damaged ECM. On day 164, this swelling has created enough radial displacement between lamellae (80%) to functionally damage elastin fibers connecting contractile VSMCs to the lamellae and thus disrupting mechanosensing. This in turn causes accelerated phenotype modulation from the contractile VSMCs to osteochodrogenic ones, and the rapid conversion—as well as lost mechanosensing and increased swelling—all work to trigger anoikis. Severe depletion of contractile VSMC population is observed in the time-frame between day 164 and the peak of elastic fibre damage at day 195. The loss in contractile VSMC population and subsequent loss of osteochondrocytes means that the abundant GAG production and natural degradative cycle of produced GAGs will see alleviated swelling and restored interlamellar spacing by day 208.

In the long term (figure 3a–d), GAG degradation through natural processes in the absence of VSMC recovery will reduce elastin fibre damage (as seen in the plateau of γ^f in panel a), but will eventually cause elastin lamellae to carry the remaining stress. That stress—in excess of homeostasis—re-triggers lamellar damage (day 354) that escalates to full degradation in the

Downloaded from http://royalsocietypublishing.org/rspa/article-pdf/doi/10.1098/rspa.2025.0787/6133611/rspa.2025.0787.pdf
by TU Delft user
on 08 May 2026

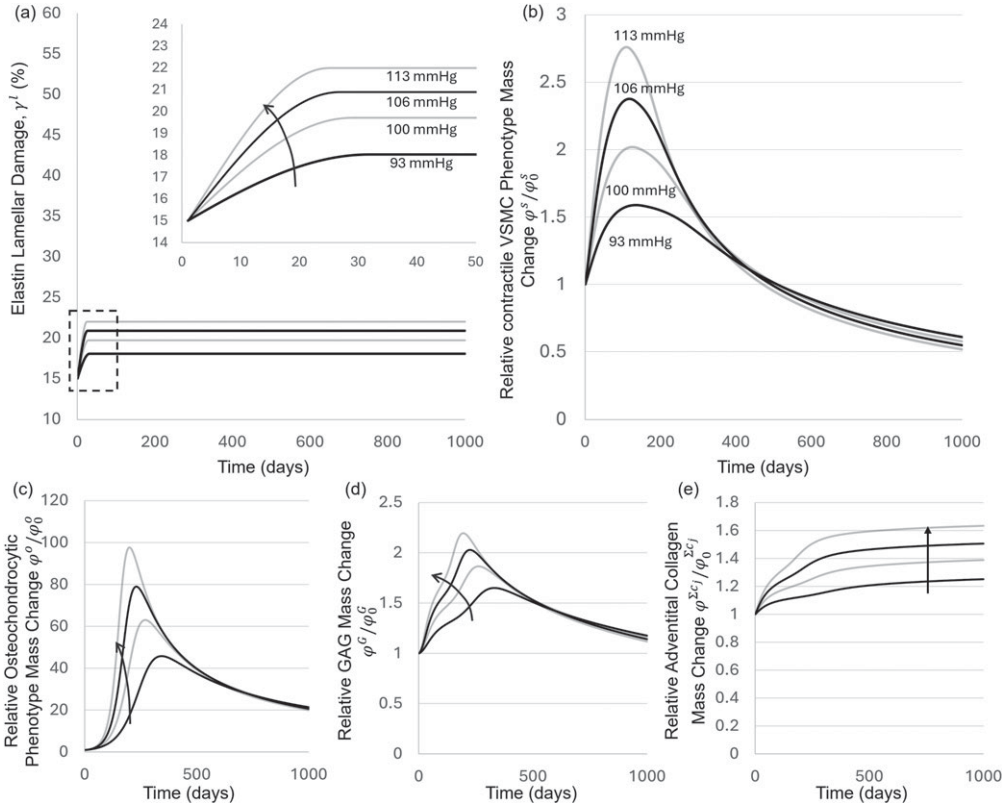

Figure 2. Evolution of relevant constituents according to our hypothesis under varying degrees of moderate hypertension. Panel (a) shows the transient damage to lamellae, and recovery due to the initial VSMC increase (b). Sustained lamellar damage, and accompanying growth of the osteochondrocytic phenotype (c) will produce excess GAGs (d). At increased degrees of hypertension, higher peaks of cell turnover are seen, but long-term restoration to equilibrium values are reached after restoration of homeostatic cell stress (trend with varying hypertension shown by black arrow). Collagen build-up in the adventitia also works to restore homeostatic stress, and increased but moderate hypertension causes increased long-term collagen deposition seen in panel (e). Simulation results shown in solid black at normotensive and hypertensive pressures of 93 mmHg and 106 mmHg, respectively, are used for comparisons in other simulations. All values are normalized from initial values, presented in electronic supplementary material, tables A.1–A.4.

absence of other load bearing constituents in the media. Moreover, panel (b) shows how the degradation of medial constituents, and compromise of elastin in particular, is compensated for by collagen buildup in the adventitia (electronic supplementary material, figure B.1). Since contractile VSMCs and elastin are the primary constituents that bear a circumferential load in the media, their depletion causes adventitial collagen to take over. Thus, elastic energy storage in our model is shown to diminish under these conditions of complete lamellar loss (as seen in panel (c)).

Our model also predicts initial inward remodelling caused by the GAG accumulation and luminal shrinkage, but with the eventual depletion of GAGs after cell loss, swelling is mitigated and the artery remodels to a homeostatic dimension (figure 4a). Therefore, it is interesting to observe that despite the similar dimensions to a physiologically healthy (homeostatic) artery, the artery is much more fibrous and less elastic as observed in tissue fibrosis.

Adventitial collagen carrying the majority of stress (shown in panels (b-d)) and characteristic loss of the bimodal s-shape of the pressure-distension curve at late stages of maladaptation (seen in electronic supplementary material, appendix B.1 figure B.2 panel (c)) are also demonstrated at severe hypertension. These fibrous arteries exhibit elevated PWVs as seen in table 1, with a PWV $> 14\,\mathrm{m\,s^{-1}}$ at day 900 post-insult.

Downloaded from http://royalsocietypublishing.org/rspa/article-pdf/doi/10.1098/rspa.2025.0787/6133611/rspa.2025.0787.pdf
by TU Delft user
on 08 May 2026

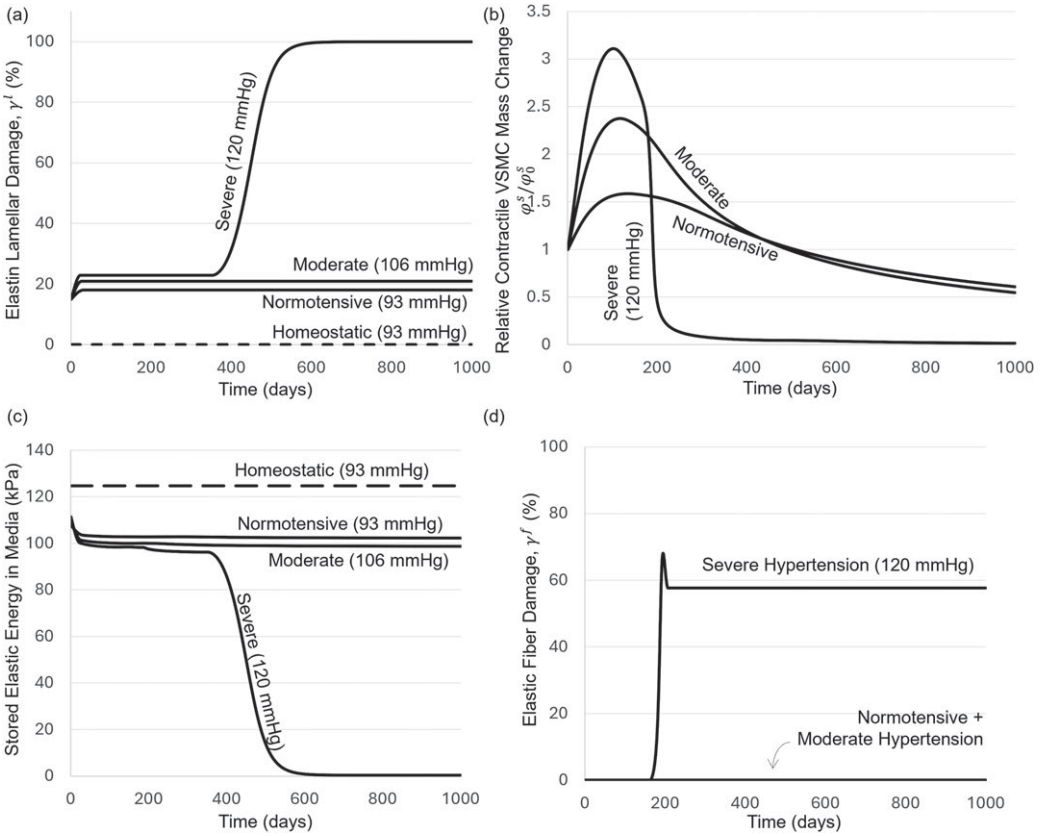

Figure 3. Evolution of relevant constituents and stored elastic energy under severe hypertension. Panel (a) informs us of the eventual medial degeneration of elastic constituents in severe hypertension. We observe the compensatory effect of GAGs on lamellae (day 0–354), having an antagonistic effect on fibers (triggered on day 164 in panel (d)). Unlike moderate hypertension, the swelling caused by these excess GAGs is enough to disrupt interlamellar elastin fibers, and mechanosensitivity is impaired as seen in panel (d). This rapidly accelerates maladaptation, and within 31 days (in the period spanning onset of mechanosensitive disruption at day 164 to stabilization on day 195) we observe complete VSMC transition and elevated cell death (b). The opposite effect appears when GAGs are depleted and the lamellae have to carry the excess loads again without shielding from VSMCs or GAGs (day 354–1000). These are primarily the radial loads since the circumferential one is accounted for with adventitial collagen increase. Panel (c) suggests that concurrent with lost cell population and lamellar degradation, the biomechanical markers observed in many pathologies of elastic arteries are also reported in our model. The loss of elastance and diminished Windkessel effect in the media of these elastic arteries has immediate consequences on artery stiffening and further complications.

(c) Scenario 3: intervention and recovery by reducing hypertension

The presented third scenario demonstrates the potential of the model/framework as a hypothesis-testing tool. Running simulations where blood pressure is restored from 120 mmHg to 93 mmHg at some point in time suggests the existence of a point-of-no-return, and we observe a gradual change in model prediction when intervening at days 94, 95 and 96 after insult. As illustrated in figure 5, minor but decreasing VSMC loss is seen at 1000 days in simulations where pressure is restored at later elapsing days post-insult but before 94 days. These arteries show no compromised mechnosensitivity in turned-over VSMCs, and thus recover similar to normotensive and moderately hypertensive arteries in **scenario 1**. (We avoid reporting all simulations of intervention before day 94, but demonstrate this extreme intervention at day 94 in figure 5 as seen by the dotted line). Contrarily, intervention at day 95 post-insult and hypertension demonstrates an intermediary recovery profile with mild VSMC loss, and sustained but halted

Downloaded from http://royalsocietypublishing.org/rspa/article-pdf/doi/10.1098/rspa.2025.0787/6133611/rspa.2025.0787.pdf
by TU Delft user
on 08 May 2026

Table 1. Table of Pulse Wave Velocity (PWV) calculated from our model. Data points are plotted in figure 7.

			PWV at Time-Points			
	Operational Pressure	Insult-free PWV	Day 0	Day 50	Day 300	Day 900
Scenario 1			Normotensive (93 mmHg)			
	Normotensive (93 mmHg)	7.249440763	8.196025	8.259756	7.67013	7.97802
			Moderate Hypertension (106 mmHg)			
	Moderate Hypertension (106 mmHg)	8.68125294	9.483349	9.365051	8.600383	9.407849
Scenario 2			Severe Hypertension (120 mmHg)			
	Severe Hypertension (120 mmHg)	10.25399295	11.13748	10.56608	10.56974	14.03421
Scenario 3			Day 94 Intervention			
	Severe Hypertension (120 mmHg)	10.25399295	11.13748	10.56608		
	Normotensive (93 mmHg)				7.725366	8.439371
			Day 95 Intervention			
	Severe Hypertension (120 mmHg)	10.25399295	11.13748	10.56608		
	Normotensive (93 mmHg)				7.572213	10.32293
			Day 96 Intervention			
	Severe Hypertension (120 mmHg)	10.25399295	11.13748	10.56608		
	Normotensive (93 mmHg)				7.991585	12.20701
Scenario 4			120 mmHg Rapid Rate			
	Severe Hypertension (120 mmHg)	10.25399295	11.13748	10.71957	9.875992	10.70073
			120 mmHg Intact Collagen			
	Severe Hypertension (120 mmHg)	10.25399295	11.13748	10.53881	9.794544	10.76819

compromise of mechanosensitivity intermediary between **scenario 1** and **scenario 2**. Finally, intervention at day 96 does not prevent eventual failure (shown in the long dashed line).

While we understand that accelerated VSMC phenotype switch happens when mechanosensing becomes compromised, this only occurs at day 164 (as seen in the §3b), and failure to recover before day 94 implies that the point-of-no-return shown in the model comes before the major cause of failure (lost mechanosensing) is triggered. There is a marked difference in response when intervention from hypertension is done early enough, where moderate recovery of cell populations can still take place and medial rescue remains possible, and thus we show that we can start with conditions similar to **scenario 2** but end with outcomes in **scenario 1** subject to intervention time.

(d) Scenario 4: intervention and recovery by enhancing adventitial response

In replicating the conditions of **scenario 2**, we observe that rapid collagen turnover supports non-homeostatic loads rapidly, alleviating growth-inducing stress on contractile VSMCs, and resulting in a smaller peak contractile VSMC mass during adaptation as seen in the dashed line in figure 6 in panel (a). This sub-critical mass, and the absence of lamellar damage (dashed in panel (b)), avoids critical osteochondrocytic phenotype build-up and cells eventually recover to an outcome similar to **scenario 1**. Furthermore, enhancing the adventitial response via maintaining deposited collagen integrity also avoids elastin lamellar damage and excess osteochondrocytic phenotype proliferation, although peak cell turnover (and thus likelihood of reaching critical mass) is larger in this strategy compared to the prior. The outcome is equally as favourable, with PWV of these

Downloaded from http://royalsocietypublishing.org/rspa/article-pdf/doi/10.1098/rspa.2025.0787/6133611/rspa.2025.0787.pdf
by TU Delft user
on 08 May 2026

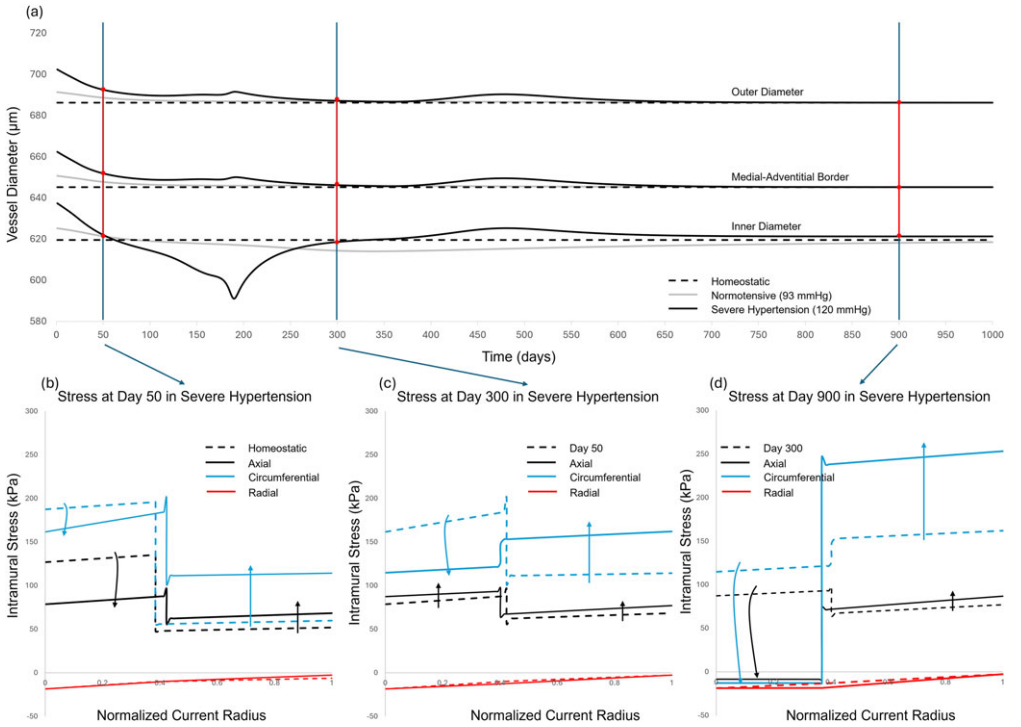

Figure 4. Evolution of *in silico* vessel dimensions and intramural wall stresses under normotension and severe hypertension. Panel (a) demonstrates the remodelling of the artery to dimensions that are similar to the homeostatic ones in the final configuration. This suggests that physiological dimensions (which were not explicitly maintained as a conserved value) with radically different biomechanical behaviour are not enough to determine disease. Assessment of intramural stress at discrete times (50 , 300 and 900 days) during maladaptation shows that concurrent with elastin loss in the media is a sizeable increase in elastic stress in the adventitia. The transition is most evident in a comparison between panels (b), (c) and (d) where the latter shows a sharp decline in circumferential and axial stresses with the loss of load-bearing constituents, and a noticeable increase in adventitial load-bearing.

arteries both showing similar or identical stiffness in late-stage adaptation that remains similar to baseline PWV at the elevated operational pressure (figure 7c).

4. Discussion

The scientific community has recently come to understand the role of VSMC plasticity and phenotype switching in aortic disease, whereby they change in morphology and function to produce GAG-dense ECM in response to perturbation from their own mechanical environments and a loss of sensitivity to that environment [2,22]. The concurrence of these phenomena in ageing and aortopathies can be partly explained through the maladaptation of cells and the consequences of this maladaptation, and can be incorporated in numerical and computational models. Capturing the interplay between these processes and their influence on one another is vital for the understanding and study of diseases and their underlying mechanisms *in silico*. What we present in this work is a model that can simulate cases of biomechanical and cellular compromise exhibited in different aortopathies, given assumptions of the underlying mechanisms, and sensible initial conditions. The model's versatility allows us to simulate cases of adaptation and irreversible maladaptation depending on the severity of the conditions mirroring clinical settings, demonstrated here via pressure-driven supra-physiological loading in presence of mild elastin damage (insult) at baseline.

Downloaded from http://royalsocietypublishing.org/rspa/article-pdf/doi/10.1098/rspa.2025.0787/6133611/rspa.2025.0787.pdf
by TU Delft user
on 08 May 2026

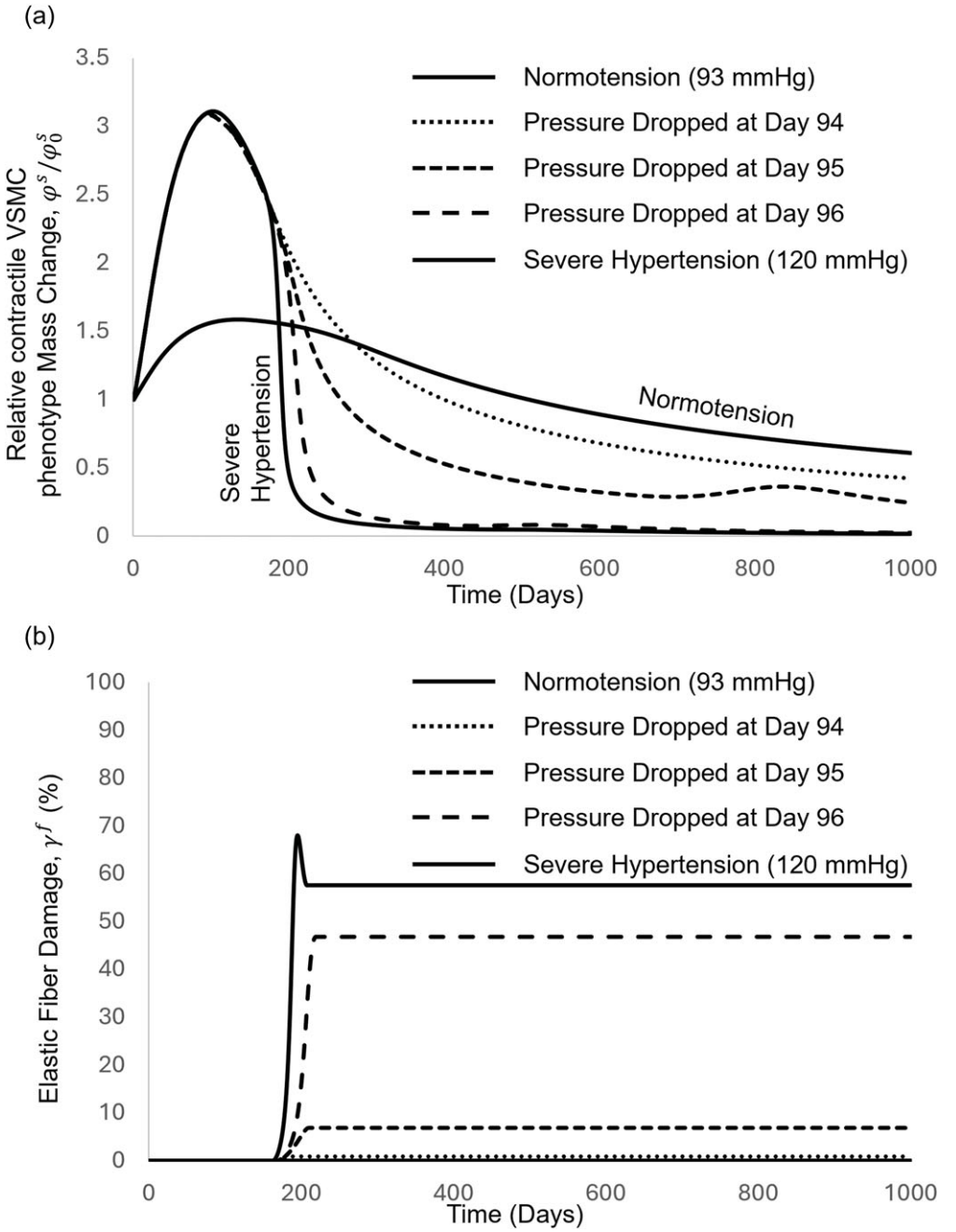

Figure 5. Evolution of contractile VSMC population and compromised mechanosensitivity at severe hypertension and interventions to normotension. A point of bifurcation appears depending on when intervention is chosen to take place. Lowering pressure from hypertensive to normotensive on day 94 (dotted line) shows outcomes of cell population recovery (panel (a)) and maintained mechanosensitivity (panel (b)) as seen in response to insult at normotension or moderate hypertension. On the other hand, intervention on day 95 (short dash) presents an intermediary response between physiological adaptation, and pathological maladaptation. Intervention at day 96 (long dash) onward suggests that the restorative process seems to have passed 'critical point' beyond which maladaptation and progressive medial degeneration take place.

(a) Model implementation and results in the context of current insights

While we are not the first to present a model that replicates arterial failure or maladaptation due to insult [33,47–49], we are confident in reporting that adaptation and maladaptation observed in our

Downloaded from http://royalsocietypublishing.org/rspa/article-pdf/doi/10.1098/rspa.2025.0787/6133611/rspa.2025.0787.pdf
by TU Delft user
on 08 May 2026

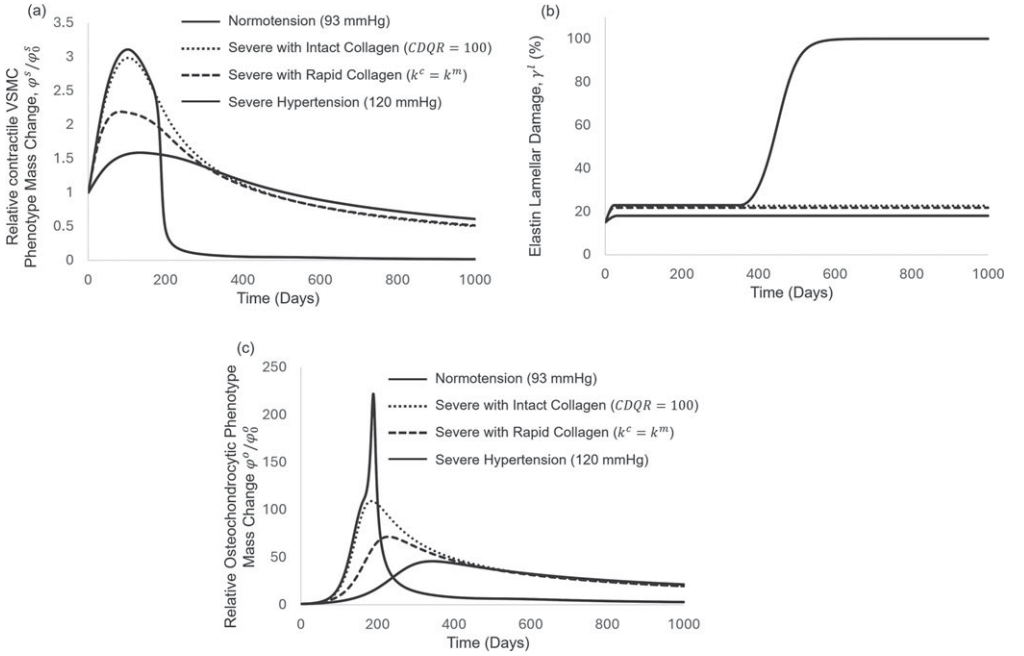

Figure 6. Evolution of contractile VSMC population, elastin lamellar damage and the osteochondrocytic phenotype population at severe hypertension with enhanced adventitial response. Rapid collagen turnover (dashed line), upon insult, reduces peak contractile VSMC turnover as seen in panel (a), preventing lamellar damage (panel (b)), and critical osteochondrocytic cell accumulation (panel (c)). Intact collagen turnover (dotted line) also prevents maladaptation, rescuing the media from crossing the 'critical point'.

model lends additional credence to the cause–effect relationship between medial degeneration, and the mechanisms for maintenance of biomechanical homeostasis. Post-insult, the model demonstrates mild loss in contractile cell population after turnover, but maintains lamellar integrity in normotensive and mildly hypertensive conditions (figure 2).

Severe hypertension (120 mmHg) stimulates large VSMC turnover initially in a disrupted ECM environment (figure 3b), and creates the intractable conditions for osteochondrocytic proliferation (panel (a) in electronic supplementary material, figure B.1) and contractile VSMC phenotype switch. While we observe rapid swelling of the media and larger VSMC, and increased GAG production in the earlier phase of severe hypertension (panel (c) in electronic supplementary material, figure B.1), this excess gives way to VSMC population collapse and GAG turnover, and thus the absence of GAG producers creates excess loading on the elastin lamellae, where we see progressive lamellar loss. This is different to the long-term response observed in moderate hypertension scenarios.

Additionally, the model is capable of reproducing significant biomechanical markers of arterial maladaptation in severe hypertension, where we show the lost elastic potential of the artery (figure 3c) as seen in clinical cases and animal models of medial degeneration [14,19,25,29]. Not only is the biomechanical profile of the maladapted arteries replicated, but the constitutive and cellular profile of diminished cells, excess GAGs and degraded elastin are similarly reported in our simulations (figure 3). We report the characteristic bimodal s-shape seen in healthy arteries in adapted arteries as evident in panel (a),(b) in electronic supplementary material, appendix B.1 figure B.2 [37]. However, in simulated maladapted arteries (panel (c)), this loss is observed at later days of maladaptation, post-medial degeneration, which is otherwise seen in elastase treated arteries [21].

The model predicts an increase in PWV upon onset of insult (Day 0) as seen in figure 7. All scenarios demonstrate the effect of the adaptive process in reducing PWV early in the process

Downloaded from http://royalsocietypublishing.org/rspa/article-pdf/doi/10.1098/rspa.2025.0787/6133611/rspa.2025.0787.pdf
by TU Delft user
on 08 May 2026

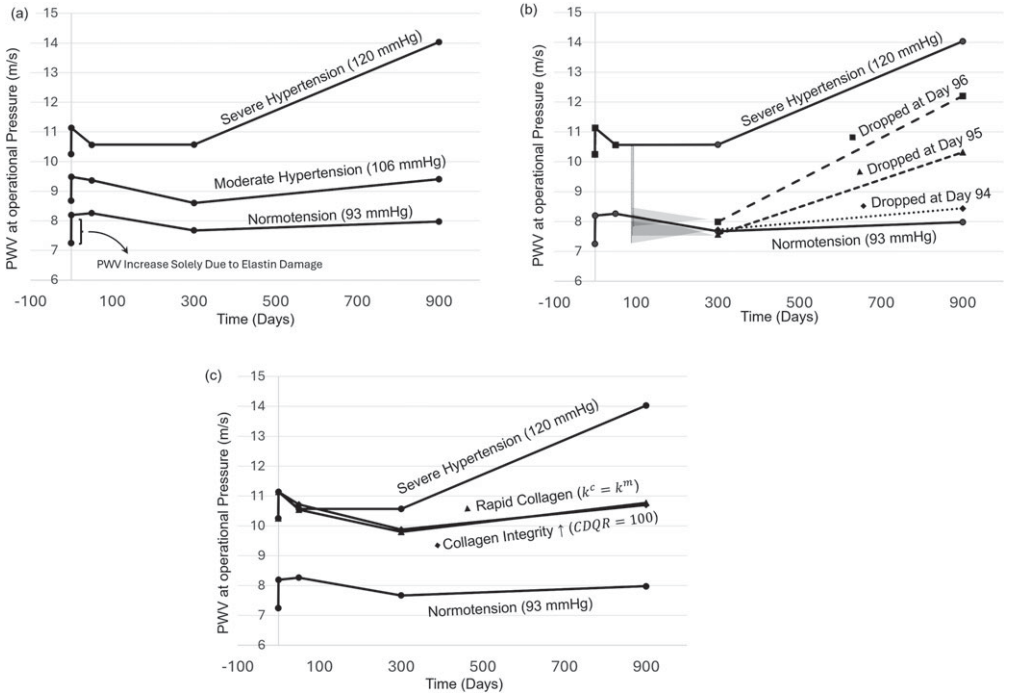

Figure 7. Pulse Wave Velocity (PWV) data reported at 4 discrete time-points in different simulated scenarios. Panel (a) demonstrates PWVs adapted under persistent normotensive, moderately hypertensive, and severely hypertensive operational pressures (**Scenario 1 & 2**). Panel (b) shows PWVs at intervened pressure from 120 mmHg done at day 94 (dotted), day 95 (short dashes) and day 96 (long dashes) (**Scenario 3**). Panel (c) shows PWV variation under severe hypertension with an enhaced adventitial response either through rapid collagen turnover (triangle) or with maintained collagen intergity (diamond) (**Scenario 4**). We emphasize that these plots are not to be read as continuous time-points, but 4 discrete readings. Panel (b) shows the discontinuity between readings as operational pressure is dropped.

(Day 50–300) towards a homeostatic value ($7.249\,\mathrm{m\,s^{-1}}$), but persistence of elevated pressures increases vessel stiffness again (Day 900) and maladaptation causes drastic stiffening (as seen in **Scenario 2**). Similarly, once intervention is taken on too late, the model predicts an eventual failure and stiffening in the long term (**Scenario 3**), while early intervention drastically eliminates a long-term effect of hypertension (dotted in **Scenario 3**). The model also highlights the importance of the adventitia on the media, showing that supplemented collagen remodelling can rescue from severe maladaptation, and avoid excess artery stiffness in the long term (**Scenario 4**).

(i) Our model in the context of hypertension

Hypertension imposes mechanical and metabolic stress on VSMCs, triggering a phenotypic switch from a contractile to a synthetic and pro-inflammatory state [50]. This transition is characterized by down-regulation of contractile phenotype biomarkers and increased cell proliferation, migration, and ECM turnover [51,52]. This state also promotes vascular remodelling and medial thickening, with chronic hypertensive stress further reprogramming contractile VSMCs into the osteochondrogenic phenotype [53], leading to active vascular calcification [54]. This calcification and remodelling results in increased arterial stiffness and pulse wave velocity (PWV), elevating systolic blood pressure and pulse pressure, while reducing diastolic perfusion [55]. The stiffened arteries further propagate mechanical stress on VSMCs, sustaining the synthetic and osteochondrogenic phenotype in a pathological feedback loop. Together, these findings establish a vicious cycle wherein hypertension drives VSMC dysfunction and vascular

Downloaded from http://royalsocietypublishing.org/rspa/article-pdf/doi/10.1098/rspa.2025.0787/6133611/rspa.2025.0787.pdf
by TU Delft user
on 08 May 2026

calcification [56], which in turn amplify vascular resistance and blood pressure [8], contributing to the progression of hypertensive cardiovascular disease.

Central to our model is that there is a preferred homeostasis that cells serve to maintain and conserve, and it was through gradual degrees of moderate hypertension, and subsequently a more severe one that we challenge this homeostasis in **scenario 1** and **scenario 2**, respectively. As such, at least some consideration should be given to what extent the model reproduces arterial remodelling in hypertension. Interrogating the impact of hypertension on maladaptation in our model successfully allowed us to distinguish between the bifurcative behaviour of arteries that exhibit mild ECM turnover but maintained biomechanical function in moderate hypertension (**scenario 1**), and maladapted arteries with excessive elastin degradation and VSMC loss in severe hypertension (**scenario 2**).

Moderate hypertension causes VSMC buildup similar to severe hypertension early on post-insult (figure 2) which triggers GAG up-regulation. The absence of excess swelling prevents ECM damage and compromised mechanosensitivity, and prevention of this critical ECM disruption, along with the preserved ability of VSMCs to sense their environment, prevents anoikis and widespread phenotype switching and suggests a similarity to many cases of GAG build-up that don't result in aggressive elastin degradation [20,26].

While **scenario 1** showed a mild response in the long term, severe hypertension provoked a detrimental response in **scenario 2**. As illustrated in figures 3 and electronic supplementary material, B.1, the model predicts severe disruption of the media in **scenario 2**, with an almost complete loss of its VSMC population and elastic function. It is remarkable that these fundamental changes occur with little noticeable change in vessel size as observed by panel (a) in figure 4. This may in part be attributed to the maintenance of adventitial integrity in our model, where we have overlooked the degradative and inflammatory processes that accelerate collagen degradation as well, similar to elastin [11]. Notwithstanding these assumptions, this demonstrates that arterial remodelling may not be captured by morphological/geometrical biomarkers typically used in clinics (e.g. to characterize dissection likelihood in aneurysms) and can only be fully understood through a more comprehensive assessment of tissue constitution [57–59].

An interesting result produced by the model is revealed in **scenario 3,** where we tested the impact of (the timing of) restoration of blood pressure to normotensive values. Simulations suggest a tipping point (94/95 days for the tested model configuration), beyond which the maladaptive cascade becomes irreversible. Unloading the artery before this point-of-no-return, however, allows the physiological collagen and contractile VSMC turnover to dominate over the phenotype switch and maladaptation. While elastic function is not restored to pre-hypertensive values, there is no complete depletion of contractile VSMCs. This difference is most evident in late stage PWVs at day 900 in normotensive pressures being significantly higher in late term intervention compared to earlier intervention (figure 7b). By dropping the pressure from severe hypertension to normotension, we eliminate the influence of strain-stiffening due to operational pressure on artery stiffness. Moreover, the progression of medial degeneration in late intervention highlights that artery stiffening observed at Day 900 isn't a result of pressure-induced strain-stiffening, but functional alteration of the artery, and the loss of the Windkessel effect. This presents a more bleak outcome when considering that day 300 readings of PWVs (taken well after intervention) indicate little difference between arteries in different scenarios, and offer little to inform of the future trajectory of adaptation or maladaptation, further highlighting the need for preemptive strategy in early intervention.

(ii) Our model in the context of ageing and genetic disease

Core to the model is arterial remodelling in response to elastin damage (an initial damage of 15% was assumed in **scenario 1–4**), which may result from ageing and/or specific genetic diseases leading to reduced integrity of elastic lamellae or fibrillar structures key to mechanotransduction. In our model, both lamellar and fibrillar damage are combined in the definition of K^{mal} in equation (2.6) using weighting terms for each. This implies an equal contribution of damage

Downloaded from http://royalsocietypublishing.org/rspa/article-pdf/doi/10.1098/rspa.2025.0787/6133611/rspa.2025.0787.pdf
by TU Delft user
on 08 May 2026

towards maladaptation—albeit at different rate—although Li *et al.* postulate that damage-driven halted mechanosensing (fibrillar damage) is more rapid and exponential [29], and that damage from ECM disruption (lamellar damage) has a more gradual linear influence on progression of maladaptation. We can rationalize a linear increase as a very slow exponential increase, but we might need to consider different analytical functions to distinguish these behaviours. There is existing work that involves either micro-structurally inspired models that could capture this heterogeneity, or cell-signal models that can inform the gene-expression and pathway activation involved in this complex process [30,60].

The structuring of our model allows us to relate its components—whether rate constants, gain parameters or constitutive relations—to physiologically relevant parameters. For example, genetic predisposition to disrupted mechanosensing (such as in MFS or vEDS) or swelling driven disrupted mechanosensing (such as in ageing or hypertension) can be emulated by adjusting the rate (or propensity) of elastin fibril damage due to radial stretch in k_γ^f (equation (2.5) and electronic supplementary material, table A.1), or by lowering the threshold for damage in $\varepsilon_{r_{\text{crit}}}$ in $\Gamma(\varepsilon_r)$. While previous work dictates that elastin would fail at a stretch of 80% [43]—the default value in our model—a discrete fibre simulation of a peel test where failure of individual fibers was at much lower stretches (5–30%) still yielded accurate numerical replication of experimental peel tests of healthy elastic media [61]. Additional model results reported in electronic supplementary material, appendix i figure B.3 show that lowering the threshold for damage ($\varepsilon_{r_{\text{crit}}}$) to take place at stretches as low as 5 % can cause maladaptation to occur even at normo-tensive pressure if there is sufficient initial insult to lamellar elastin. This aligns with the possible predisposition to early maladaptation in genetic diseases increasing that susceptibility to damage [14].

Our model also allows us to investigate the role of adventitial rescue in hypertension in conditions that may be otherwise impaired in genetic diseases such as vEDS. By demonstrating that enhanced collagen remodelling can rescue at severe hypertensions (**scenario 4**), we also conclude that collagen compromise can pose a greater risk at more moderate and even normotensive pressures.

(iii) Our model in the context of aneurysms and aortic dissection

While only showcased for an elastic artery model subjected to elevated blood pressure, our proposed remodelling framework is particularly applicable to aortic aneurysms, where histopathology suggests a major compromise in its elastic and load-bearing function [10,11]. Furthermore, studies of the make-up and structure of these arteries reveals swelling and mucoid buildup due to the presence of PGs/GAGs in otherwise healthy specimens [19,26]. Additionally, the pioneering work of Glagov has shown that GAGs are used by certain cell populations as a response to cyclic disruption from homeostatic stress in their environment, suggesting a maintenance mechanism by which their presence acts [3].

At the same time, none of the simulated scenarios leads to long-term dilatation, which is experimentally observed in, for instance, elastase treated arteries [21] or BAPN + elastase treated arteries [19], where radical changes in radii and thickness are observed. The most apt comparison would therefore be a comparison with results immediately after the initial insult is applied in our simulations, which does show arterial dilatation. Inward remodelling instead of dilatation of the outer diameter is also a possible explanation, since adventitial collagen recruitment at these pressures is at its highest and is not under compromise as demonstrated by the BAPN + elastase study. Evidence of the model presented by Li *et al.* suggests that both elastin and collagen compromise are necessary for dilatation [29], and the adequate adjustment of collagen compromise to reflect this will be explored in future work.

The importance of accurately representing turned-over collagen rates or compromised quality presents us with two parameters of the model that have critical outcomes on model predictions. The parameter describing the rate of VSMC production due to stress perturbation (k^m from

Downloaded from http://royalsocietypublishing.org/rspa/article-pdf/doi/10.1098/rspa.2025.0787/6133611/rspa.2025.0787.pdf
by TU Delft user
on 08 May 2026

equation (2.6)) and that describing the rate of circumferential collagen buildup due to stress perturbation (k^{c_2} from equation (2.10)) are inextricably linked. So long as $k^m > k^{c_2}$ (as implemented in **scenario 1,2** and **3**), the recovery of circumferential function of lost elastin is taken by VSMCs, which are inherently susceptible to phenotype switch due to this initial damage. Conversely, if the rate of collagen turnover is equal or more rapid (simulated in **scenario 4**), then insult will be recovered with the intact adventitial turnover and any excess VSMCs will always recover, albeit to lower steady-state equilibrium values (similar to what is observed in physiological recovery). The quality of produced collagen will suffer from this increased rate, but no critical damage will be reached and no cell loss accompanied by elastin disintegration will occur. Similarly, if the quality of collagen remains intact, then medial rescue is still observed.

If collagen in tissues has a more rapid rate of turnover, we see this as a limiting factor in our model. However, we can rationalize this discrepancy in a few different ways. Firstly, we can assume that the rate at which collagen turnover will be accelerated can indeed be faster, but the threshold or setpoint at which this accelerated rate takes place is higher (i.e. the range of stress at which homeostasis and collagen turnover is produced is higher).

We also believe that the results of our model hold key importance in the understanding of aortic dissection and the underlying conditions that might trigger it. If the incidence of dissection occurs due to dehiscence of elastin lamellae, and luminal intrusion of blood into the media, the considerations of interlamellar stresses is crucial to determining the likelihood of that dehiscence. Our model reports medial stresses that suggest swelling and tensile osmotic forces within the media in the later stages of our simulations (panel (d) in electronic supplementary material, figure B.1) where elastin is largely absent, and thus unable to offer the necessary balance between radial compression from the new configuration and tensional buildup from swelling. This is experimentally confirmed in peeling tests where the absence of GAGs necessitated larger forces to peel apart elastin lamellae (although this was done on healthy lamellae, not fragmented ones with excess swelling) [61]. This falls within the broader conversation of the good, the bad and the ugly roles of GAGs in radial load bearing balanced with elastin radial load bearing mentioned before [31]. In physiological conditions, the media is compressed (from the lumen pushing it outward but also from the adventitia and parenchymal tissue inward, resisting deformation). In swelling, the endogenous osmotic load in the media acts against this, and in moderate amounts it is cooperative with elastin, shielding it from damage as seen in electronic supplementary material, figure B.1 panel (d), when GAGs have become hypotonic as governed by electronic supplementary material, equation A.14. In the absence of elastin, the loads become tensile, which would facilitate arterial wall delamination.

(b) Considerations on our framework

While the model presented extends the constrained mixture growth and remodelling framework by including VSMC phenotype switching and GAGs, we invite the reader to consider a few key considerations that may have an impact on our results.

A first consideration is in regard to the absence of the primary function of contractile VSMC phenotypes in active contraction and the myogenic response of active force generation in hypertension. Indeed, increased hypertensive loading in a renal artery ligation animal model is known to be accommodated in elastic arteries with increased VSMC tone in the first days after ligation until remodelling takes place [55]. The consequence of that on our model would be a diminished circumferential stress felt by the contractile VSMCs. There is more recent work, however, that suggests densification of contractile VSMCs in response to hypertension [62], which supports our construction of the model where active proliferation of cells and an increase in their numbers (mass) occurs as a response to insult.

The absence of inelastic growth from our model may also lead us to overestimate stresses on the tissue constituents, exaggerating the rates of adaptation/maladaptation. This may also explain the similarity in dimensions after maladaptation as seen in figure 4a. It is for this reason that formulations of remodelling often involve remodelled stretches $\mathbf{F}_g^{-1}$ (as seen in [41,63,64])

Downloaded from http://royalsocietypublishing.org/rspa/article-pdf/doi/10.1098/rspa.2025.0787/6133611/rspa.2025.0787.pdf
by TU Delft user
on 08 May 2026

that, when multiplied by the total deformation $\mathbf{F}(t)$ (see figure 1), will diminish the stress due to deformation. In the case of our model, incorporating it into the growth laws will move equilibrium configurations away from the homeostatic one, but this adds another dimension of complexity as we have no intuitive method by which to design this particular constitutive behaviour. When assuming a proportional non-elastic growth in swollen deformations, we observe a dampened effect and mitigation of likelihood of maladaptation as seen in electronic supplementary material, appendix i in figure B.4. This dampening aligns with the description of in-elastic growth characterized in other works [64], but generally speaking, determining that proportion offers an additional parameter that is difficult to identify in our model.

The natural turnover cycle of VSMCs [25], their senescence in ageing [65], or their change in gene-expression profiles [30,60] were not accounted for explicitly. When working with the time scales in question and forecasting over such long periods, these considerations come into question. Typically, versican is the commonly occurring PG/GAG molecule in healthy and remodelling arteries, with its distribution along the aortic tree correlating with that of elastin (decreasing from the heart to the venous system) [10,19,40]. On the other hand, expression and abundance of aggrecan is increased in aneurysms and dissections [10,11,19,22]. If versican and aggrecan have different swelling properties or mechanical ones, it can be used to distinguish between their populations and consider their distribution given the segment of the artery being modelled.

Finally, our choice to model elastin loss and mechanosensing deserves some scrutiny in how we chose not to include the detailed mechanisms by which mechanosensing is established in the first place, and how newly proliferated VSMCs produce de novo elastin [66,67], a precursor to the larger cross-linked elastin fibers along with Fibronectin, Fibrillin-4 and Fibulin fibers. Additionally, many cell phenotypes including VSMCs have self-regulating mechanosensing mechanisms, where Focal Adhesion maturation strengthens the sensing established by cells and stabilize mechanosensing and signal transduction against loss or damage of external force sensors [42]. This bears relevance to highlight that the resilience of elastin fibrils assumed in our model, or that lost mechanosensing arising from their damage, must be considered if these stabilizers occur more rapidly or more effectively.

In regards to phenotype modulation, we have chosen not to model the synthetic/degradative VSMC phenotype explicitly [2,11,23]. There is growing evidence suggesting engagement of inflammatory pathways, and modulation of the contractile phenotype to the degradative one in severe hypertension [68]. This phenotype is responsible for an up-regulation of ECM altering molecules such as matrix metalloproteases (MMPs) that have a degradative effect on ECM components (such as MMP-2, MMP-3 and MMP-12 and their degradative function on elastin and collagen) [10,11]. This can appear in three distinct roles in our model: the further depletion of contractile VSMCs (by adding an additional depletion term in equation (2.6)), the elevated rate of degradation of elastin lamellae/fibers (similarly in equations (2.3) and (2.5)), and the elevated degradation rate of collagen fibers (equation (2.10)). It may be worth exploring how these rates can be coupled to an extra phenotype population similar to how the GAGs were coupled to the population of the contractile and osteochondrogenic phenotypes. The assumption regarding contractile VSMC phenotype switch incorporated only osteochondrocytes, and not the myriad of other phenotypes that also have an effect on the ECM [2,35]. Calcification observed in many aneurysmal hypertensive artery walls with the osteochondrocytic phenotype [35] include plaque formations and fibrinogen deposits (all due to aberrant phenotypes and all with significant biomechanical characteristics overlooked here [69]). An expansion of the constrained mixture accommodating these constituents with phenotypic modulation can be used to study atherosclerotic tissue similar to previous studies [70].

(c) Limitations of our framework and future directions

The reader is provided a deeper discussion on the limitations and future directions in the extended discussion. We comment on the choice of tissue being the common carotid artery,

Downloaded from http://royalsocietypublishing.org/rspa/article-pdf/doi/10.1098/rspa.2025.0787/6133611/rspa.2025.0787.pdf
by TU Delft user
on 08 May 2026

and the considerations of our findings on other tissues, noting that many studies we build on gain their insights from other large elastic arteries, not just the CCA. We similarly comment on the choices of models we build on, and offer brief suggestions for paths forward to explore the robustness of our model further. Finally, we briefly mention possible avenues for *in vitro* validation of our simulated mechanisms using organ-on-a-chip systems.

5. Concluding remarks

In conclusion, we present in this work a model of biomechanical maladaptation. We report the ability of the models to simulate medial degeneration, cell loss and stored energy decrease—all signs of arterial dysfunction in ageing and connective tissue genetic diseases—in sustained severe hypertension and with modest initial ECM degradation. The model also simulates physiological responses in milder cases of initial damage, and the importance of timely intervention in prevention of maladaptation. The proposed model incorporates GAG dysregulation and VSMC turnover due to different stimuli and perturbation from homeostatically conserved values, relating severe changes in these environments to lost mechanosensitivity and subsequent phenotype switching. While most of this work is based on decades of experimental and theoretical soft tissue modelling, we hope to present the community with novel interpretation of the constantly shifting physiological norm dictated by evolution of the biomechanical, cellular and extra-cellular environment. By assuming the method by which this evolution takes place (phenotype switch) and what triggers this evolution, and showing that these assumptions replicate features seen in arterial dysfunction, we hope to expand the general body of work in this field. It remains imperative to move closer to an understanding of the dynamic nature of adaptation and the feedback loops that ultimately falter or cause progressive degeneration.

Data accessibility. All necessary data and code required to run, test, and reproduce simulated results are provided (https://github.com/yousofma/Data_RSPA_ABDELRAOUF).

The data are provided in electronic supplementary material [71].

Declaration of AI use. We have not used AI-assisted technologies in creating this article.

Authors' contributions. Y.MA.A.: conceptualization, formal analysis, investigation, methodology, software, visualization, writing—original draft, writing—review and editing; L.M.: methodology, writing—review and editing; L.M.: methodology, writing—review and editing; J.DB.: investigation, writing—review and editing; P.S.: investigation, writing—review and editing; M.P.: methodology, supervision, writing—review and editing; N.F.: methodology, supervision, writing—review and editing; J.D.H.: conceptualization, investigation, writing—review and editing; P.S.: conceptualization, funding acquisition, investigation, project administration, resources, supervision, writing—review and editing.

All authors gave final approval for publication and agreed to be held accountable for the work performed therein.

Conflict of interest declaration. We declare we have no competing interests.

Funding. Research was partly funded by a Concerted Action Grant of Ghent University (GOA.2021.0005.05). The work also received funding from the European Union under grant no. 101136728 (VITAL project).

Acknowledgements. We would also like to acknowledge David S. Li and Jonathan Weissmann for their valuable feedback and insightful discussions, and Sara Roccabianca for sharing the code we built upon, and the valuable perspectives she shared.

References

1. Humphrey JD. 2008 Vascular adaptation and mechanical homeostasis at tissue, cellular, and sub-cellular levels. *Cell Biochem. Biophys.* **50**, 53–78. (doi:10.1007/s12013-007-9002-3)
2. Humphrey JD, Dufresne ER, Schwartz MA. 2014 Mechanotransduction and extracellular matrix homeostasis. *Nat. Rev. Mol. Cell Biol.* **15**, 802–812. (doi:10.1038/nrm3896)
3. Glagov S, Clark JM, Leung DYM, Mathews MB. 1977 Functional relations among cells and fibers of the aortic media: microanatomic and biosynthetic findings, In *Atherosclerosis IV* (eds G Schettler, Y Goto, Y Hata, G Klose), pp. 362–365. Berlin; Heidelberg: Springer-Verlag. (doi:10.1007/978-3-642-95308-8_77)

Downloaded from http://royalsocietypublishing.org/rspa/article-pdf/doi/10.1098/rspa.2025.0787/6133611/rspa.2025.0787.pdf
by TU Delft user
on 08 May 2026

4. Karnik SK, Brooke BS, Bayes-Genis A, Sorensen L, Wythe JD, Schwartz RS, Keating MT, Li DY. 2003 A critical role for elastin signaling in vascular morphogenesis and disease. *Development* **130**, 411–423. (doi:10.1242/dev.00223)
5. Cardamone L, Valentín A, Eberth JF, Humphrey JD. 2009 Origin of axial prestretch and residual stress in arteries. *Biomech. Model. Mechanobiol.* **8**, 431–446. (doi:10.1007/s10237-008-0146-x)
6. Cocciolone AJ, Hawes JZ, Staiculescu MC, Johnson EO, Murshed M, Wagenseil JE. 2018 Elastin, arterial mechanics, and cardiovascular disease. *Am. J. Physiol. Heart Circ. Physiol.* **315**, H189–H205. (doi:10.1152/ajpheart.00087.2018.-Large)
7. Devos DG, Rietzschel E, Heyse C, Vandemaele P, Bortel LV, Babin D, Segers P, Westenberg JM, Achten R. 2015 MR pulse wave velocity increases with age faster in the thoracic aorta than in the abdominal aorta. *J. Magn. Reson. Imaging* **41**, 765–772. (doi:10.1002/jmri.24592)
8. Chirinos JA, Segers P, Hughes T, Townsend R. 2019 Large-artery stiffness in health and disease: JACC state-of-the-art review. *J. Am. Coll. Cardiol.* **74**, 1237–1263. (doi:10.1016/j.jacc.2019.07.012)
9. Tsamis A, Krawiec JT, Vorp DA. 2013 Elastin and collagen fibre microstructure of the human aorta in ageing and disease: a review. *J. R. Soc. Interface* **10**, 20121004. (doi:10.1098/rsif.2012.1004)
10. Jana S, Hu M, Shen M, Kassiri Z. 2019 Extracellular matrix, regional heterogeneity of the aorta, and aortic aneurysm. *Exp. Mol. Med.* **51**, 1–15. (doi:10.1038/s12276-019-0286-3)
11. Ganizada BH *et al.* 2024 Unveiling cellular and molecular aspects of ascending thoracic aortic aneurysms and dissections. *Basic Res. Cardiol.* **119**, 371–395. (doi:10.1007/s00395-024-01053-1)
12. Wagenseil JE, Mecham RP. 2012 Elastin in large artery stiffness and hypertension. *J. Cardiovasc. Transl. Res.* **5**, 264–273. (doi:10.1007/s12265-012-9349-8)
13. Kucherenko MM *et al.* 2023 Elastin stabilization prevents impaired biomechanics in human pulmonary arteries and pulmonary hypertension in rats with left heart disease. *Nat. Commun.* **14**, 4416. (doi:10.1038/s41467-023-39934-z)
14. Cavinato C, Chen M, Weiss D, Ruiz-Rodríguez MJ, Schwartz MA, Humphrey JD. 2021 Progressive microstructural deterioration dictates evolving biomechanical dysfunction in the Marfan aorta. *Front. Cardiovasc. Med.* **8**, 800730. (doi:10.3389/fcvm.2021.800730)
15. Vatner SF, Zhang J, Vyzas C, Mishra K, Graham RM, Vatner DE. 2021 Vascular stiffness in aging and disease. *Front. Physiol.* **12**, 762437. (doi:10.3389/fphys.2021.762437)
16. Ooshima A, Fuller GC, Cardinale GJ, Spector S, Udenfriend S. 1974 Increased collagen synthesis in blood vessels of hypertensive rats and its reversal by antihypertensive agents (prolyl hydroxylase/hypertension/reserpine). *Proc. Natl Acad. Sci. USA* **71**, 3019–3023. (doi:10.1073/pnas.71.8.3019)
17. Carmo M, Colombo L, Bruno A, Corsi FRM, Roncoroni L, Cuttin MS, Radice F, Mussini E, Settembrini PG. 2002 Alteration of elastin, collagen and their cross-links in abdominal aortic aneurysms. *Eur. J. Vasc. Endovasc. Surg.* **23**, 543–549. (doi:10.105/ejvs.2002.1620)
18. Kawamura Y, Murtada SI, Gao F, Liu X, Tellides G, Humphrey JD. 2021 Adventitial remodeling protects against aortic rupture following late smooth muscle-specific disruption of TGFβ signaling. *J. Mech. Behav. Biomed. Mater.* **116**, 104264. (doi:10.1016/j.jmbbm.2020.104264)
19. Weiss D, Latorre M, Rego BV, Cavinato C, Tanski BJ, Berman AG, Goergen CJ, Humphrey JD. 2021 Biomechanical consequences of compromised elastic fiber integrity and matrix cross-linking on abdominal aortic aneurysmal enlargement. *Acta Biomater.* **134**, 422–434. (doi:10.1016/j.actbio.2021.07.059)
20. Yousef S *et al.* 2021 Quantitative not qualitative histology differentiates aneurysmal from nondilated ascending aortas and reveals a net gain of medial components. *Sci. Rep.* **11**, 13185. (doi:10.1038/s41598-021-92659-1)
21. Ferruzzi J, Collins MJ, Yeh AT, Humphrey JD. 2011 Mechanical assessment of elastin integrity in fibrillin-1-deficient carotid arteries: implications for Marfan syndrome. *Cardiovasc. Res.* **92**, 287–295. (doi:10.1093/cvr/cvr195)
22. Koch CD, Lee CM, Apte SS. 2020 Aggrecan in cardiovascular development and disease. *J. Histochem. Cytochem.* **68**, 777–795. (doi:10.1369/0022155420952902)
23. Gkousioudi A, Sigaeva T, Yu X, Seta F, Wainford RD, Zhang Y. 2023 Compromised homeostasis in aged carotid arteries revealed by microstructural studies of elastic lamellae. *J. Mech. Behav. Biomed. Mater.* **148**, 106187. (doi:10.1016/j.jmbbm.2023.106187)

Downloaded from http://royalsocietypublishing.org/rspa/article-pdf/doi/10.1098/rspa.2025.0787/6133611/rspa.2025.0787.pdf
by TU Delft user
on 08 May 2026

24. Cavinato C, Murtada SI, Rojas A, Humphrey JD. 2021 Evolving structure-function relations during aortic maturation and aging revealed by multiphoton microscopy. *Mech. Ageing Dev.* **196**, 111471. (doi:10.1016/j.mad.2021.111471)
25. Murtada SI, Kawamura Y, Cavinato C, Wang M, Ramachandra AB, Spronck B, Li DS, Tellides G, Humphrey JD. 2023 Biomechanical and transcriptional evidence that smooth muscle cell death drives an osteochondrogenic phenotype and severe proximal vascular disease in progeria. *Biomech. Model. Mechanobiol.* **22**, 1333–1347. (doi:10.1007/s10237-023-01722-5)
26. Eliathamby D, Keshishi M, Ouzounian M, Forbes TL, Tan K, Simmons CA, Chung J. 2023 Ascending aortic geometry and its relationship to the biomechanical properties of aortic tissue. In *JTCVS open*, vol. 13, pp. 32–44. Boston, MA: Elsevier B.V. (doi:10.1016/j.xjon.2022.08.015)
27. Eberth JF, Gresham VC, Reddy AK, Popovic N, Wilson E, Humphrey JD. 2009 Importance of pulsatility in hypertensive carotid artery growth and remodeling. *J. Hypertens.* **27**, 2010–2021. (doi:10.1097/HJH.0b013e32832e8dc8)
28. Eberth JF, Popovic N, Gresham VC, Wilson E, Humphrey JD. 2010 Time course of carotid artery growth and remodeling in response to altered pulsatility. *Am. J. Physiol. Heart Circ. Physiol.* **299**, H1875–H1883. (doi:10.1152/ajpheart.00872.2009.-Eluci)
29. Li DS, Cavinato C, Latorre M, Humphrey JD. 2023 Computational modelling distinguishes diverse contributors to aneurysmal progression in the Marfan aorta. *Proc. R. Soc. A* **479**, 20230116. (doi:10.1098/rspa.2023.0116)
30. Maes L, Vervenne T, Hoof LV, Jones EA, Rega F, Famaey N. 2023 Computational modeling reveals inflammation-driven dilatation of the pulmonary autograft in aortic position. *Biomech. Model. Mechanobiol.* **22**, 1555–1568. (doi:10.1007/s10237-023-01694-6)
31. Roccabianca S, Bellini C, Humphrey JD. 2014 Computational modelling suggests good, bad and ugly roles of glycosaminoglycans in arterial wall mechanics and mechanobiology. *J. R. Soc. Interface* **11**, 20140397. (doi:10.1098/rsif.2014.0397)
32. Sorrentino TA, Fourman L, Ferruzzi J, Miller KS, Humphrey JD, Roccabianca S. 2015 Local versus global mechanical effects of intramural swelling in carotid arteries. *J. Biomech. Eng.* **137**, 041008. (doi:10.1115/1.4029303)
33. Murtada SI *et al.* 2020 Paradoxical aortic stiffening and subsequent cardiac dysfunction in Hutchinson–Gilford progeria syndrome. *J. R. Soc. Interface* **17**, 20200066. (doi:10.1098/rsif.2020.0066)
34. Yahagi K, Kolodgie FD, Lutter C, Mori H, Romero ME, Finn AV, Virmani R. 2017 Pathology of human coronary and carotid artery atherosclerosis and vascular calcification in diabetes mellitus. *Arterioscler. Thromb. Vasc. Biol.* **37**, 191–204. (doi:10.1161/ATVBAHA.116.306256)
35. Durham AL, Speer MY, Scatena M, Giachelli CM, Shanahan CM. 2018 Role of smooth muscle cells in vascular calcification: implications in atherosclerosis and arterial stiffness. *Cardiovasc. Res.* **114**, 590–600. (doi:10.1093/cvr/cvy010)
36. Humphrey JD, Rajagopal KR. 2002 A constrained mixture model for growth and remodeling of soft tissues. *Math. Models Methods Appl. Sci.* **12**, 407–430. (doi:10.1142/S0218202502001714)
37. Bellini C, Ferruzzi J, Roccabianca S, Martino ESD, Humphrey JD. 2014 A microstructurally motivated model of arterial wall mechanics with mechanobiological implications. *Ann. Biomed. Eng.* **42**, 488–502. (doi:10.1007/s10439-013-0928-x)
38. Ateshian GA. 2007 On the theory of reactive mixtures for modeling biological growth. *Biomech. Model. Mechanobiol.* **6**, 423–445. (doi:10.1007/s10237-006-0070-x)
39. Ateshian GA, Albro MB, Maas S, Weiss JA. 2011 Finite element implementation of mechanochemical phenomena in neutral deformable porous media under finite deformation. *J. Biomech. Eng.* **133**, 081005. (doi:10.1115/1.4004810)
40. Azeloglu EU, Albro MB, Thimmappa VA, Ateshian GA, Costa KD. 2008 Heterogeneous transmural proteoglycan distribution provides a mechanism for regulating residual stresses in the aorta. *Am. J. Physiol. Heart Circ. Physiol.* **294**, H1197–H1205. (doi:10.1152/ajpheart.01027.2007)
41. Latorre M, Humphrey JD. 2018 A mechanobiologically equilibrated constrained mixture model for growth and remodeling of soft tissues. *Z. Angew. Math. Mech.* **98**, 2048–2071. (doi:10.1002/zamm.201700302)
42. Ribeiro-Silva JC, Miyakawa AA, Krieger JE. 2021 Focal adhesion signaling: vascular smooth muscle cell contractility beyond calcium mechanisms. *Clin. Sci.* **135**, 1189–1207. (doi:10.1042/CS20201528)

Downloaded from http://royalsocietypublishing.org/rspa/article-pdf/doi/10.1098/rspa.2025.0787/6133611/rspa.2025.0787.pdf
by TU Delft user
on 08 May 2026

43. Lillie MA, Gosline JM. 2007 Limits to the durability of arterial elastic tissue. *Biomaterials* **28**, 2021–2031. (doi:10.1016/j.biomaterials.2007.01.016)
44. Stanton H, Melrose J, Little CB, Fosang AJ. 2011 Proteoglycan degradation by the ADAMTS family of proteinases. *Biochim. Biophys. Acta (BBA)—Mol. Basis Dis.* **1812**, 1616–1629. (doi:10.1016/j.bbadis.2011.08.009)
45. Inc. TM. 2023 MATLAB version: 23.2.0.2365128 (R2023b).
46. Segers P, Chirinos JA. 2022 Arterial wall stiffness: basic principles and methods of measurement in vivo. In *Textbook of arterial stiffness and pulsatile hemodynamics in health and disease*, pp. 111–124. London, UK: Elsevier. (doi:10.1016/B978-0-323-91391-1.00007-8)
47. Mahutga RR, Barocas VH. 2020 Investigation of pathophysiological aspects of aortic growth, remodeling, and failure using a discrete-fiber microstructural model. *J. Heat Transfer* **142**, 111007. (doi:10.1115/1.4048031)
48. Rachev A, Shazly T. 2019 A structure-based constitutive model of arterial tissue considering individual natural configurations of elastin and collagen. *J. Mech. Behav. Biomed. Mater.* **90**, 61–72. (doi:10.1016/j.jmbbm.2018.09.047)
49. Ahmadzadeh H, Rausch MK, Humphrey JD. 2019 Modeling lamellar disruption within the aortic wall using a particle-based approach. *Sci. Rep.* **9**, 15320. (doi:10.1038/s41598-019-51558-2)
50. Jensen LF, Bentzon JF, Albarrán-juárez J. 2021 The phenotypic responses of vascular smooth muscle cells exposed to mechanical cues. *Cells* **10**, 2209. (doi:10.3390/cells10092209)
51. Cao G, Xuan X, Hu J, Zhang R, Jin H, Dong H. 2022 How vascular smooth muscle cell phenotype switching contributes to vascular disease. *Cell Commun. Signal.* **20**, 180. (doi:10.1186/s12964-022-00993-2)
52. Swiatlowska P *et al.* 2022 Pressure and stiffness sensing together regulate vascular smooth muscle cell phenotype switching. *Sci. Adv.* **8**, 3471. (doi:10.1126/sciadv.abm3471)
53. Xin Y, Zhang Z, Lv S, Xu S, Liu A, Li H, Li P, Han H, Liu Y. 2024 Elucidating VSMC phenotypic transition mechanisms to bridge insights into cardiovascular disease implications. *Front. Cardiovasc. Med.* **11**, 1400780. (doi:10.3389/fcvm.2024.1400780)
54. Iyemere VP, Proudfoot D, Weissberg PL, Shanahan CM. 2006 Vascular smooth muscle cell phenotypic plasticity and the regulation of vascular calcification. *J. Intern. Med.* **260**, 192–210. (doi:10.1111/j.1365-2796.2006.01692.x)
55. Trachet B, Bols J, Degroote J, Verhegghe B, Stergiopulos N, Vierendeels J, Segers P. 2015 An animal-specific FSI model of the abdominal aorta in anesthetized mice. *Ann. Biomed. Eng.* **43**, 1298–1309. (doi:10.1007/s10439-015-1310-y)
56. den Bergh GV, Opdebeeck B, D'Haese PC, Verhulst A. 2019 The vicious cycle of arterial stiffness and arterial media calcification. *Trends Mol. Med.* **25**, 1133–1146. (doi:10.1016/j.molmed.2019.08.006)
57. Polzer S, Gasser TC. 2015 Biomechanical rupture risk assessment of abdominal aortic aneurysms based on a novel probabilistic rupture risk index. *J. R. Soc. Interface* **12**, 20150852. (doi:10.1098/rsif.2015.0852)
58. Linden KV *et al.* 2023 Stiffness matters: improved failure risk assessment of ascending thoracic aortic aneurysms. *JTCVS Open* **16**, 66–83. (doi:10.1016/j.xjon.2023.09.008)
59. Gheysen L, Maes L, Caenen A, Segers P, Peirlinck M, Famaey N. 2024 Uncertainty quantification of the wall thickness and stiffness in an idealized dissected aorta. *J. Mech. Behav. Biomed. Mater.* **151**, 106370. (doi:10.1016/j.jmbbm.2024.106370)
60. Irons L, Humphrey JD. 2020 Cell signaling model for arterial mechanobiology. *PLoS Comput. Biol.* **16**, e1008161. (doi:10.1371/journal.pcbi.1008161)
61. Yu X, Suki B, Zhang Y. 2020 Avalanches and power law behavior in aortic dissection propagation. *Sci. Adv.* **6**, eaaz1173 (doi:10.1126/sciadv.aaz1173)
62. Hayashi K, Shimizu E. 2016 Composition of connective tissues and morphometry of vascular smooth muscle in arterial wall of DOCA-salt hypertensive rats—in relation with arterial remodeling. *J. Biomech.* **49**, 1225–1229. (doi:10.1016/j.jbiomech.2016.02.044)
63. Cyron CJ, Aydin RC, Humphrey JD. 2016 A homogenized constrained mixture (and mechanical analog) model for growth and remodeling of soft tissue. *Biomech. Model. Mechanobiol.* **15**, 1389–1403. (doi:10.1007/s10237-016-0770-9)
64. Braeu FA, Seitz A, Aydin RC, Cyron CJ. 2017 Homogenized constrained mixture models for anisotropic volumetric growth and remodeling. *Biomech. Model. Mechanobiol.* **16**, 889–906. (doi:10.1007/s10237-016-0859-1)

Downloaded from http://royalsocietypublishing.org/rspa/article-pdf/doi/10.1098/rspa.2025.0787/6133611/rspa.2025.0787.pdf
by TU Delft user
on 08 May 2026

65. Chi C, Li DJ, Jiang YJ, Tong J, Fu H, Wu YH, Shen FM. 2019 Vascular smooth muscle cell senescence and age-related diseases: state of the art. *JCI Insight* **1865**, 1810–1821. (doi:10.1016/j.bbadis.2018.08.015)
66. Hassab AH, Hur DJ, Vallabhajosyula P, Tellides G, Assi R. 2024 Intimomedial tears of the aorta heal by smooth muscle cell-mediated fibrosis without atherosclerosis. *JCI Insight* **9**, e172437. (doi:10.1172/jci.insight.172437)
67. Ellis MW *et al.* 2024 De novo elastin assembly alleviates development of supravalvular aortic stenosis—brief report. *Arterioscler. Thromb. Vasc. Biol.* **44**, 1674–1682. (doi:10.1161/ATVBAHA.124.320790)
68. Estrada AC, Humphrey JD. 2025 Multi-scale multi-cell computational model of inflammation-mediated aortic remodeling in hypertension. *Ann. Biomed. Eng.* **53**, 1014–1023. (doi:10.1007/s10439-025-03685-3)
69. Harman JL, Jørgensen HF. 2019 The role of smooth muscle cells in plaque stability: therapeutic targeting potential. *Br. J. Pharmacol.* **176**, 3741–3753. (doi:10.1111/bph.14779)
70. Gierig M, Tragoudas A, Haverich A, Wriggers P. 2024 Mechano-chemo-biological model of atherosclerosis formation based on the outside-in theory. *Biomech. Model. Mechanobiol.* **23**, 539–552. (doi:10.1007/s10237-023-01790-7)
71. Abdel-Raouf YMA, Maes L, Maga L, De Backer J, Sips P, Peirlinck M, Famaey N, Humphrey JD, Segers P. 2026 The role of vascular smooth muscle cell plasticity in arterial remodelling and biomechanical failure: a numerical approach. Figshare. (doi:10.6084/m9.figshare.c.8351677)

Downloaded from http://royalsocietypublishing.org/rspa/article-pdf/doi/10.1098/rspa.2025.0787/6133611/rspa.2025.0787.pdf
by TU Delft user
on 08 May 2026